

# The heavy neutral Higgs signature in the $\gamma\gamma \rightarrow ZZ$ process.<sup>†</sup>

G.J. Gounaris<sup>a</sup>, P.I. Porfyriadis<sup>a</sup> and F.M. Renard<sup>b</sup>

<sup>a</sup>Department of Theoretical Physics, Aristotle University of Thessaloniki,  
 Gr-54006, Thessaloniki, Greece.

<sup>b</sup>Physique Mathématique et Théorique, UMR 5825  
 Université Montpellier II, F-34095 Montpellier Cedex 5.

## Abstract

If the Standard Model (SM) Higgs particle is sufficiently heavy, then its contribution to  $\gamma\gamma \rightarrow ZZ$  should be largely imaginary, interfering with the also predominantly imaginary SM "background" generated by the  $W$ -loop. For standard model Higgs masses in the region  $200 \lesssim m_H \lesssim 500$  GeV, this interference is found to be constructive and increasing the Higgs signal. In the minimal SUSY case an interference effect should also appear for the contribution of the heavier CP-even neutral Higgs boson  $H^0$ , provided it is sufficiently heavy. The effect is somewhat reduced though, by the smallness of the  $H^0$  width and the  $\gamma\gamma$  and  $ZZ$  branching ratios. The interference is again found to be constructive for part of the parameter space corresponding to sfermion masses at the TeV scale and maximal stop mixing. For both the SM and SUSY cases, regions of the parameter space exist though, where the interference may be destructive. It is therefore essential to take these effects into account when searching for possible scalar Higgs-like candidates. To this aim, we present the complete analytic expressions for both resonance and background amplitudes.

---

<sup>†</sup>Partially supported by the European Community grant HPRN-CT-2000-00149.

# 1 Introduction

Searching for the Higgs particle(s) is definitely the central aim in particle physics at present. If the Standard Model (SM) correctly describes nature, then the present LEP results require the Higgs mass to be heavier than 113 GeV [1]. This constraint is somewhat loosened in minimal SUSY, in which for typical scenarios assuming sfermion masses at the TeV scale and maximal stop mixing, the lower bound on the mass of the lightest CP-even neutral Higgs  $h^0$  is reduced to about 90 GeV, while the  $\tan\beta$ -region ( $0.5 - 2.3$ ) is excluded [1].

After the discovery of the Higgs particle(s), the necessity will of course arise to secure its identification. To this aim, a photon-photon Collider ( $LC_{\gamma\gamma}$ ) realized through the laser backscattering method [2] in a high luminosity  $e^-e^-$  or  $e^+e^-$  Collider (LC) [3], should be very useful. In an  $LC_{\gamma\gamma}$  the neutral Higgs particle may then be produced directly in the  $s$ -channel, and if it is not too narrow, even its line shape may be studied.

For a standard model (SM) light Higgs boson (i.e.  $m_H \lesssim 135$  GeV) the rate of direct production in  $\gamma\gamma \rightarrow H$  is indeed very high and the detection of the Higgs boson should clearly be done through the dominant decay channel  $H \rightarrow b\bar{b}$  [4, 5, 6]. For higher Higgs masses though, the situation changes because the Higgs becomes broader and the dominant channels are now  $WW$  and  $ZZ$ . A very interesting channel for Higgs detection is then the  $ZZ$  one, in which at least one  $Z$  decays into lepton pairs and the other one into hadrons or leptons. Such a channel will be very interesting, even though  $Br(H \rightarrow \gamma\gamma)$  decreases rapidly as the Higgs mass increases.

However, to this  $\gamma\gamma \rightarrow H \rightarrow ZZ$  channel, there is an important  $\gamma\gamma \rightarrow ZZ$  background process arising mainly through  $W$  and fermions box-type contributions [7, 8, 9]. As it has already been noticed in [10] from the study of strong  $WW$  interactions, it is possible to enhance the signal relative to the background by using polarized photon beams and applying suitable cuts on the decay products of the  $Z$  bosons.

But, as emphasized in [9], this background process has the remarkable property that at high energies its predominant helicity amplitudes are almost purely imaginary and conserve helicity<sup>1</sup>. Thus, important interference effects between the Higgs and background contributions may appear, which should be taken into account when analyzing experimental data.

The first aim of this paper is to explore this interference phenomenon in SM for Higgs masses above the  $ZZ$  production threshold, using the already known one-loop  $\gamma\gamma \rightarrow ZZ$  amplitudes [7, 8, 9].

We next turn to a general MSSM model [13], assuming no CP violation other than the standard one contained in the Yukawa sector. In this case, the Higgs boson spectrum is much richer, with two CP-even scalars  $h^0$ ,  $H^0$  and one CP-odd pseudoscalar  $A^0$  [14]. We consider SUSY scenarios in which  $H^0$  and  $A^0$  are heavier than about 200 GeV, while the SUSY breaking sfermion parameters are taken at the TeV scale and the stop mixing is maximal. Such scenarios have the tendency to lead to an  $h^0$  which is well within the

---

<sup>1</sup>A similar property has also been observed for the processes  $\gamma\gamma \rightarrow \gamma\gamma$ ,  $\gamma Z$  at sufficiently high energies [11, 12].

presently experimentally allowed region [1]. The lightest Higgs boson vertex  $h^0\gamma\gamma$  for SUSY models, has recently been studied in [15]. Since the CP-odd  $A^0$  has no tree-level coupling to  $\gamma\gamma$  or  $ZZ$ , the  $\gamma\gamma \rightarrow ZZ$  channel may be used for the on-shell production of the CP-even Higgs  $H^0$ .

Apart from the existence of the lighter Higgs  $h^0$ , there are several new features discriminating the heavier SUSY  $H^0$  boson, from the case of a heavy standard Higgs. The decay spectrum of the SUSY  $H^0$  is expected to differ from that of a heavy standard Higgs, because of the possible appearance of new decay channels and mixing effects which strongly influence its couplings to gauge bosons. Thus for  $m_{H^0} \gtrsim 200\text{GeV}$ , the SUSY  $H^0$  is expected to be much narrower than a heavy standard  $H$ , and its branching ratios  $Br(H^0 \rightarrow \gamma\gamma)$  and  $Br(H^0 \rightarrow ZZ)$  much smaller [14, 16]. Moreover, in an MSSM description, the  $\gamma\gamma \rightarrow ZZ$  background receives at one loop new contributions from virtual SUSY partners running inside the loop [9]. So finally, within the MSSM, the treatment of the Higgs effects in the  $\gamma\gamma \rightarrow ZZ$  process requires a specific analysis. This constitutes the second topic of this paper.

In Section 2 we write the Higgs contributions to the  $\gamma\gamma \rightarrow ZZ$  amplitudes for the SM ( $H$ ) and for the MSSM ( $h^0$ ,  $H^0$ ) cases. We give the explicit expressions of the one loop Higgs couplings to  $\gamma\gamma$  and the tree level couplings to  $ZZ$ . In the Appendix we collect all background amplitudes for  $\gamma\gamma \rightarrow ZZ$  in SM and in MSSM. They are taken from [9], except for the mixed chargino box contributions arising when two different charginos are running along the box loop, which had not been computed before. In Section 3 we compute the polarized  $\gamma\gamma \rightarrow ZZ$  differential cross section induced by the above Higgs and background contributions. We discuss the shape of the  $ZZ$  invariant mass distribution and the observability of the Higgs signal, in particular its dependence on the photon-photon flux for polarized laser photon and  $e^\pm$  beams. We show that, for a given Higgs mass, it is possible to optimize the configuration by varying either the LC energy or the energy of the laser beam. We give various illustrations with heavy SM and MSSM Higgs particles. The results are summarized and commented in the concluding Section 4.

## 2 The Higgs contribution to the $\gamma\gamma \rightarrow ZZ$ amplitudes.

As in [9, 11, 12], we use the non-linear Feynman gauge in which there are two sets of diagrams contributing to  $\gamma\gamma \rightarrow ZZ$  [17]; compare Fig.1. The first consists of the one-particle irreducible "box"-diagrams involving two photons and two  $Z$ 's as external legs; see Fig.1a. Their contributions, arising from loops involving  $W$ 's [8], quarks and leptons and charginos [7], as well as charged Higgs particles and sfermions [9], are summarized in the Appendix. We note in particular that the "mixed" chargino boxes, induced by the  $Z\tilde{\chi}_1\tilde{\chi}_2$  couplings involving two different charginos, are presented in (A.36, A.51-A.66). Numerically, they are not expected to be particularly important. Nevertheless, we list them here for completeness, because their derivation (including their simplification to the present form) required a considerable effort. The analogous "mixed" sfermion box

contributions have not been calculated, since they should be at most of similar magnitude to the single sfermion, which is already known to be very small [9].

The second set of diagrams<sup>2</sup> depicted in Fig.1b, consists of those involving contributions from a Higgs pole in the  $\hat{s}$ -channel. These diagrams contain a Higgs- $\gamma\gamma$  vertex generated by loops along which  $W$ -gauge bosons (together with the associated Goldstone and FP ghosts) and fermion or physical scalar particles are running. Their general form is

$$F_{\lambda_1\lambda_2\lambda_3\lambda_4}^h(\gamma\gamma \rightarrow ZZ) = -\frac{\alpha^2}{2s_W^2 c_W^2} \left\{ \mathcal{H}(\hat{s}) \right\} \cdot \frac{(1 + \lambda_1\lambda_2)}{2} \left[ (1 + \lambda_3\lambda_4) \frac{\lambda_3\lambda_4}{2} - \frac{1 + \beta_Z^2}{1 - \beta_Z^2} (1 - \lambda_3^2)(1 - \lambda_4^2) \right], \quad (1)$$

where the hyperfine coupling is taken as  $\alpha = 1/137$ .

In SM, where only one physical neutral Higgs particle exists with mass  $m_H$ , we have

$$\mathcal{H}(\hat{s}) = \sum_i N_i^c Q_i^2 \mathcal{F}_i(\tilde{\tau}) \frac{\hat{s}}{\hat{s} - m_H^2 + im_H \Gamma_H}, \quad (2)$$

where the index  $i$  runs over the physical charged particles with spin (1, 1/2) running along the loop with their interactions determined by [14]

$$\mathcal{L}_{H^0(SM)} = gm_W W_\mu^+ W^{\mu-} H^0 - \frac{gm_f}{2m_W} \bar{\psi}_f \psi_f H^0 - \frac{gm_H^2}{2m_W} G^+ G^- H^0, \quad (3)$$

where  $G^\pm$  are the standard model Goldstone bosons associated to the  $W^\pm$  bosons. The  $W$  (plus Goldstone and FP ghost) and the charged fermion contributions to  $H^0\gamma\gamma$  are given respectively by

$$\mathcal{F}_1(\tilde{\tau}) = \frac{2m_H^2}{\hat{s}} + 3\tilde{\tau} + 3\tilde{\tau} \left( \frac{8}{3} - \frac{2m_H^2}{3\hat{s}} - \tilde{\tau} \right) f(\tilde{\tau}), \quad (4)$$

$$\mathcal{F}_{1/2}(\tilde{\tau}) = -2\tilde{\tau}[1 + (1 - \tilde{\tau})f(\tilde{\tau})], \quad (5)$$

where

$$\tilde{\tau} = \frac{4m_i^2}{\hat{s}}, \quad f(\tilde{\tau}) = -\frac{\hat{s}}{2} C_0(0, 0, \hat{s}; m_i, m_i, m_i), \quad (6)$$

with<sup>3</sup>  $C_0$  being the standard Passarino-Veltman function [18] in the notation of [9, 19]; (compare (A.37-A.46)). In (2),  $Q_i$  is the charge and  $N_i^c$  the colour multiplicity of the particle contributing to  $H^0\gamma\gamma$  loop.

The most important contributions to (2) in SM come from  $W^\pm$  (to which Goldstone and FP ghost are always included) and the top-loop, which are determined by (4) and (5) respectively.

<sup>2</sup>Notice that as opposed to the previous set, these are one-particle reducible diagrams.

<sup>3</sup>A simple expression for  $C_0$  in terms of logarithms may be seen *e.g.* in Eqs.(B.2) of [9].

It is also useful to remark that if a physical scalar charged particle  $H^\pm$  with mass  $m_{H^\pm}$  were introduced in SM interacting with the physical neutral Higgs as [14]

$$\mathcal{L}_{H^0 H^+ H^-} = -\frac{gm_{H^\pm}^2}{m_W} H^+ H^- H^0, \quad (7)$$

then an additional contribution would arise in (2) determined by the function

$$\mathcal{F}_0(\tilde{\tau}) = \tilde{\tau}[1 - \tilde{\tau}f(\tilde{\tau})], \quad (8)$$

which is analogous to those in (4, 5) and determines the contributions to  $H\gamma\gamma$  from spin=0 charged particles running along the loop [14]. Using this, it may then be instructive to notice that the standard  $W^\pm$  contribution (4) can be written as

$$\mathcal{F}_1(\tilde{\tau}) = 3\tilde{\tau} \left[ 1 + \left( \frac{8}{3} - \tilde{\tau} \right) f(\tilde{\tau}) \right] + \frac{m_H^2}{2m_W^2} \mathcal{F}_0(\tilde{\tau}). \quad (9)$$

In the Feynman gauge, the first term in (9) gives the pure  $W$  and ghost SM contributions, while the last term (having exactly the structure that would be induced by a scalar charge=1 particle of mass  $m_W$ ) describes the Goldstone one. But of course, such a separation is not gauge invariant.

In the MSSM case, with no CP-violating phases in the new physics sector, there will be two neutral CP-even Higgs particles ( $h^0$ ,  $H^0$ ) contributing to (1) so that

$$\begin{aligned} \mathcal{H}(\hat{s}) = & \sum_i N_i^c Q_i^2 \left[ \sin(\beta - \alpha) \mathcal{F}_i^{h^0}(\tilde{\tau}) \frac{\hat{s}}{\hat{s} - m_{h^0}^2 + im_{h^0} \Gamma_{h^0}} \right. \\ & \left. + \cos(\beta - \alpha) \mathcal{F}_i^{H^0}(\tilde{\tau}) \frac{\hat{s}}{\hat{s} - m_{H^0}^2 + im_{H^0} \Gamma_{H^0}} \right], \end{aligned} \quad (10)$$

where the sum is running over the physical charged particles with spin (1, 1/2, 0) contributing to the  $h^0\gamma\gamma$  and  $H^0\gamma\gamma$  vertices; these are  $W^\pm$  (to which  $G^\pm$  and FP ghosts are always included), as well as charginos  $\tilde{\chi}^\pm$ ,  $H^\pm$  and sfermions  $\tilde{f}_j$ . The interaction Lagrangian determining the necessary couplings is

$$\begin{aligned} \mathcal{L}_{(h^0, H^0)(\text{SUSY})} = & gm_W [H^0 \cos(\beta - \alpha) + h^0 \sin(\beta - \alpha)] \left\{ W^{-\mu} W_\mu^+ + \frac{1}{2c_W^2} Z^\mu Z_\mu - H^+ H^- \right\} \\ & + \frac{gm_W}{2c_W^2} \cos 2\beta [h^0 \sin(\alpha + \beta) - H^0 \cos(\alpha + \beta)] (G^+ G^- - H^+ H^-) \\ & - \frac{gm_t}{2m_W \sin \beta} [H^0 \sin \alpha + h^0 \cos \alpha] \bar{t} t - \frac{g}{2m_W \cos \beta} [H^0 \cos \alpha - h^0 \sin \alpha] (m_b \bar{b} b + m_\tau \bar{\tau} \tau) \\ & - \frac{gm_t^2}{m_W \sin \beta} [h^0 \cos \alpha + H^0 \sin \alpha] (\tilde{t}_1^* \tilde{t}_1 + \tilde{t}_2^* \tilde{t}_2) - \frac{gm_t}{2m_W \sin \beta} [h^0 (A_t \cos \alpha + \mu \sin \alpha) \\ & + H^0 (A_t \sin \alpha - \mu \cos \alpha)] \sin(2\theta_t) \text{Sign}(A_t - \mu \cot \beta) (\tilde{t}_1^* \tilde{t}_1 - \tilde{t}_2^* \tilde{t}_2) \end{aligned}$$

$$\begin{aligned}
& -\frac{gm_W}{c_W^2}[H^0 \cos(\alpha + \beta) - h^0 \sin(\alpha + \beta)] \left\{ \left[ \frac{2s_W^2}{3} + \left( \frac{1}{2} - \frac{4s_W^2}{3} \right) \cos^2 \theta_t \right] \tilde{t}_1^* \tilde{t}_1 \right. \\
& + \left. \left[ \frac{2s_W^2}{3} + \left( \frac{1}{2} - \frac{4s_W^2}{3} \right) \sin^2 \theta_t \right] \tilde{t}_2^* \tilde{t}_2 \right\} \\
& - \frac{g}{\sqrt{2}} \tilde{\Delta}_1 \left[ \tilde{\mathcal{B}}_L \cos \phi_R \sin \phi_L (H^0 \cos \alpha - h^0 \sin \alpha) + \tilde{\mathcal{B}}_R \sin \phi_R \cos \phi_L (H^0 \sin \alpha + h^0 \cos \alpha) \right] \tilde{\chi}_1 \tilde{\chi}_1 \\
& + \frac{g}{\sqrt{2}} \tilde{\Delta}_2 \left[ \tilde{\mathcal{B}}_R \sin \phi_R \cos \phi_L (H^0 \cos \alpha - h^0 \sin \alpha) \right. \\
& + \left. \tilde{\mathcal{B}}_L \sin \phi_L \cos \phi_R (H^0 \sin \alpha + h^0 \cos \alpha) \right] \tilde{\chi}_2 \tilde{\chi}_2 .
\end{aligned} \tag{11}$$

The implied  $W$ -loop contributions to the  $h^0$ ,  $H^0$  terms in (10) are then respectively

$$\mathcal{F}_1^{h^0}(\tilde{\tau}) = \sin(\beta - \alpha) 3\tilde{\tau} \left[ 1 + \left( \frac{8}{3} - \tilde{\tau} \right) f(\tilde{\tau}) \right] - \frac{\cos(2\beta) \sin(\beta + \alpha)}{2c_W^2} \mathcal{F}_0(\tilde{\tau}) , \tag{12}$$

$$\mathcal{F}_1^{H^0}(\tilde{\tau}) = \cos(\beta - \alpha) 3\tilde{\tau} \left[ 1 + \left( \frac{8}{3} - \tilde{\tau} \right) f(\tilde{\tau}) \right] + \frac{\cos(2\beta) \cos(\beta + \alpha)}{2c_W^2} \mathcal{F}_0(\tilde{\tau}) , \tag{13}$$

while the contributions from fermion and physical scalar particles are given by (5, 8) respectively, after substituting of course the obvious changes in the couplings implied by comparing (3, 7) with (11).

Concerning the parameters entering (11), we quote the neutral Higgs mixing angle  $\alpha$  determined by [13]

$$\tan(2\alpha) = \tan(2\beta) \frac{m_{A^0}^2 + m_Z^2}{m_{A^0}^2 - m_Z^2 + \frac{\epsilon}{\cos(2\beta)}} , \tag{14}$$

and the constraint  $-\pi/2 \leq \alpha \leq 0$ . The leading top-stop contribution to (14) is [20]

$$\epsilon \simeq \frac{3G_F m_t^4}{\sqrt{2}\pi^2 \sin^2 \beta} \ln \left( \frac{M_S^2}{m_t^2} \right) , \tag{15}$$

where  $M_S^2 \simeq m_{\tilde{t}_1} m_{\tilde{t}_2}$  provides a measure of the SUSY breaking scale.

We also note that the neutral Higgs- $\tilde{t}_i$  couplings in (11) depend on the  $(\tilde{t}_L, \tilde{t}_R)$  mixing defined in (A.19, A.18); while the neutral Higgs-chargino couplings in (11), assume the mixing definition in (A.26-A.30) and the sign quantities  $\tilde{\Delta}_1$ ,  $\tilde{\Delta}_2$ ,  $\tilde{\mathcal{B}}_L$  and  $\tilde{\mathcal{B}}_R$  given in (A.35). The consistency of the formalism guarantees that the chargino physical masses are always positive, for any sign of  $M_2$  and  $\mu$ .

### 3 The $\gamma\gamma \rightarrow ZZ$ process close to the Higgs pole.

We now explore the possibility of studying the contribution of a Higgs  $s$ -channel pole using polarized  $\gamma\gamma$  collisions in an LC operated in the  $\gamma\gamma$  mode, through laser backscattering [2]. With Bose statistics and Parity invariance the general form for the  $\gamma\gamma \rightarrow ZZ$  cross section has been written in [9] for any polarization state of the photons, in terms of

helicity amplitudes. Here we restrict to the case of circular laser polarization (without any transverse linear part) which turns out to be most interesting for the search of Higgs effects. The cross section for the laser backscattered photons normalized to unit electron positron flux is then [9]

$$\left. \frac{d\sigma(\gamma\gamma \rightarrow ZZ)}{dw d\cos\vartheta^*} \right|_{\text{Laser}} = \frac{1}{\sqrt{s_{ee}}} \frac{d\bar{L}_{\gamma\gamma}}{d\sqrt{\tau}} \left\{ \frac{d\bar{\sigma}_0}{d\cos\vartheta^*} + \langle \xi_2 \xi'_2 \rangle \frac{d\bar{\sigma}_{22}}{d\cos\vartheta^*} \right\} , \quad (16)$$

where  $w \equiv \sqrt{s_{\gamma\gamma}} \equiv \sqrt{\hat{s}}$  is the c.m. energy of the backscattered photons, equal to the  $ZZ$  invariant mass, while  $\sqrt{s_{ee}}$  is the  $e^-e^+$  c.m. energy at which the LC is operating. The relevant  $\gamma\gamma$  cross sections are given by

$$\frac{d\bar{\sigma}_0(\gamma\gamma \rightarrow ZZ)}{d\cos\vartheta^*} = \left( \frac{\beta_Z}{128\pi\hat{s}} \right) \sum_{\lambda_3\lambda_4} [|F_{++\lambda_3\lambda_4}|^2 + |F_{+-\lambda_3\lambda_4}|^2] , \quad (17)$$

$$\frac{d\bar{\sigma}_{22}(\gamma\gamma \rightarrow ZZ)}{d\cos\vartheta^*} = \left( \frac{\beta_Z}{128\pi\hat{s}} \right) \sum_{\lambda_3\lambda_4} [|F_{++\lambda_3\lambda_4}|^2 - |F_{+-\lambda_3\lambda_4}|^2] , \quad (18)$$

in terms of helicity amplitudes defined in Appendix A. In (16-18),  $\vartheta^*$  denotes the Z-scattering angle in  $\gamma\gamma$  c.m. frame. Note that  $d\bar{\sigma}_0/d\cos\vartheta^*$  is the unpolarized  $\gamma\gamma \rightarrow ZZ$  cross section and therefore it is positive definite, while  $d\bar{\sigma}_{22}/d\cos\vartheta^*$  can be of either sign. In terms of these, the cross section for case that both photons have helicity=+1, is expressed as

$$\frac{d\bar{\sigma}_{++}(\gamma\gamma \rightarrow ZZ)}{d\vartheta^*} = \frac{d\bar{\sigma}_0(\gamma\gamma \rightarrow ZZ)}{d\vartheta^*} + \frac{d\bar{\sigma}_{22}(\gamma\gamma \rightarrow ZZ)}{d\vartheta^*} . \quad (19)$$

The quantity  $d\bar{L}_{\gamma\gamma}/d\sqrt{\tau}$  in (16) describes the photon-photon differential luminosity per unit  $e^-e^+$  (or  $e^-e^-$ ) flux at  $\tau \equiv s_{\gamma\gamma}/s_{ee}$ ; while the Stokes parameters  $\xi_2, \xi'_2$  describe the helicities of the two backscattered photons [2], so that  $\langle \xi_2 \xi'_2 \rangle$  denote the average value of the product of these helicities as a function of  $\tau$ . Here, we follow the same notation as in [2, 21] and the Appendix B of the last paper in [11].

As explained in [2], after the Compton scattering of an electron beam of energy  $E$  from a laser photon of energy  $\omega_0$ , the electron loses most of its energy and a beam of "backscattered photons" is produced with the energy  $\omega$ , whose fractional energy  $x \equiv \omega/E$  satisfies

$$0 \leq x \leq x_{max} \equiv \frac{x_0}{1+x_0} \quad , \quad 0 \leq x_0 \leq 2(1+\sqrt{2}) \quad , \quad (20)$$

where  $x_0 = 4E\omega_0/m_e^2$ . Applying laser backscattering to both electron beams, we conclude that the c.m. energy of the produced hard photons is constrained by

$$\tau < \frac{x_0 x'_0}{(1+x_0)(1+x'_0)} \quad , \quad (21)$$

where we have allowed for the possibility that the energies of the two laser photons may be different.

It turns out that the shapes of  $d\bar{L}_{\gamma\gamma}/d\sqrt{\tau}$  and  $\langle\xi_2\xi'_2\rangle$  strongly depend also on the longitudinal polarizations of the two electron beams  $P_e$  and  $P'_e$  and on the average helicities of the corresponding laser photons  $P_\gamma$  and  $P'_\gamma$ . Examples of these are shown in Fig.2a,b, for the most interesting case  $P_e = P'_e = 0.8$ ,  $P_\gamma = P'_\gamma = -1$  in which both  $d\bar{L}_{\gamma\gamma}/d\sqrt{\tau}$  and  $\langle\xi_2\xi'_2\rangle$  peak at a  $\tau$ -value close to the maximum allowed by (21). Thus for the highest possible value of  $x_0 = x'_0 = 4.83$ , this peak appears at  $\sqrt{\tau} \simeq 0.8$  where  $\langle\xi_2\xi'_2\rangle \simeq 1$ . By varying  $(x_0, x'_0)$ , for a given LC energy  $E_e$ , it should be possible to move the peak of these distributions at the value of the mass of the Higgs boson one wants to study, thereby increasing the sensitivity; compare Fig.2a,b. In Fig.2c, the photon-photon Luminosity factor for unpolarized electron and laser beams are given for comparison. As discussed below, under certain circumstances it may be advisable to use such unpolarized beams in the Higgs searches!

We now examine how the distribution in eq.(16) can reflect the presence of a Higgs boson and allow to study its properties. In this respect the contributions from the diagrams of Fig.1b determine the "signal", while those of Fig.1a the " $\gamma\gamma \rightarrow ZZ$ -background".

In a first step we fix the energy of the  $e^+e^-$  LC to its maximal value, for example at 500 GeV or 800 GeV for the TESLA project [22, 23]. For the SM Higgs boson case, we then look at the effect for Higgs masses at 200, 300, 400 and 500 GeV<sup>4</sup>. As a second step, depending on the situation, we can improve the sensitivity by either optimizing the choice of the  $(x_0, x'_0)$  values, or the LC machine energy. Below, we discuss examples of both situations.

### **SM cases:**

As expected from the shapes of the luminosity factors  $d\bar{L}_{\gamma\gamma}/d\sqrt{\tau}$  and  $\langle\xi_2\xi'_2\rangle$  presented in Fig.2a,b, if  $x_0 = 4.83$ , then the Higgs effect will be mostly visible in the case of a Higgs mass corresponding to  $\sqrt{\tau_H} \equiv m_H/\sqrt{s_{ee}} \simeq 0.8$ , i.e.  $m_H \simeq 400$  GeV for a 500 GeV LC machine.

We start therefore from this  $m_H = 400$  GeV case presented in Fig.3, where the laser induced cross section defined in (16) is plotted versus  $\sqrt{\tau}$ . The total Higgs width used in the calculation is obtained from the code of [24] and it is indicated in Fig.3. In the same figure the results for  $m_H = 100$  GeV are also given as a help for estimating the background. Note that the cross sections are always integrated in the  $30^\circ < \vartheta^* < 150^\circ$  angular region.

It is evident from Fig.3 that the magnitude of the  $m_H = 400$  GeV contribution, compared to the background, is maximized in a region which is not symmetric around the  $\sqrt{s_{\gamma\gamma}} = 400$  GeV region. This must be related to energy region where the signal-background interference is most constructive; as well as to the shape of the photon spectrum and the magnitude of the Higgs width.

---

<sup>4</sup>We note in passing that standard model Higgs masses of up to 500 GeV, or even larger, may easily be made consistent with all experimental data and theoretical bounds, by either introducing new very heavy particles or extra large dimension. For a review see [27].

Using (16), the expected number of events in some appropriate region of  $ZZ$  invariant masses  $w_{\min} < w < w_{\max}$  around the Higgs pole is then defined by

$$\mathcal{N}^{\text{SM}} = \mathcal{L}_{ee} I_f \int_{w_{\min}}^{w_{\max}} dw \frac{d\sigma}{dw d\cos\vartheta^*} \Big|_{\text{Laser}}, \quad (22)$$

$$\mathcal{N}_{\text{Bg}}^{\text{SM}} = \mathcal{L}_{ee} I_f \int_{w_{\min}}^{w_{\max}} dw \frac{d\sigma(m_H = 100\text{GeV})}{dw d\cos\vartheta^*} \Big|_{\text{Laser}}, \quad (23)$$

for the signal and the background respectively. Here  $\mathcal{L}_{ee}$  is the LC luminosity which for 0.5TeV TESLA LC is taken  $\mathcal{L}_{ee} = 300 \text{ fb}^{-1}/\text{year}$  at its top energy [23]. From (22, 23), the statistical significance of the effect is then given by

$$S.D. \equiv \frac{(\mathcal{N}^{\text{SM}} - \mathcal{N}_{\text{Bg}}^{\text{SM}})}{\sqrt{\mathcal{N}_{\text{Bg}}^{\text{SM}}}}. \quad (24)$$

The quantity  $I_f$  in (22, 23) denotes the identification factor of the  $Z$ -pair. Assuming that the useful modes for the  $ZZ$  identification are those where one  $Z$  decays leptonically (including the invisible neutrino mode), and the other hadronically, we get  $I_f \simeq 0.47$ ; while if only charged leptons are used for the leptonic mode,  $I_f \simeq 0.14$  is obtained. In the following we will present event-numbers and statistical significance corresponding to both cases,  $I_f = 0.47$  and in parenthesis  $I_f = 0.14$ .

Thus, for the SM case of  $m_H = 400\text{GeV}$ , (presented in Fig.3) we get, the results indicated in the second column of Table 1. Of course the results mildly depend also on the choice of  $ZZ$  invariant masses  $w_{\min}$  and  $w_{\max}$  which, on the basis of Fig.3, have been taken asymmetrically around the Higgs mass. This choice is also indicated in Table 1. The conclusion thus reached is that the sensitivity of a 0.5 TeV LC to a  $m_H = 400\text{GeV}$  SM Higgs seems to be quite high.

We next turn to lower Higgs masses. If we insist using for them  $x_0 = x'_0 = 4.83$  with the beams polarized as in Figs.2a,b and  $\sqrt{s_{ee}} = 0.5\text{TeV}$ , then the effect will be weaker, because of the smaller values of the luminosity factor  $d\bar{L}_{\gamma\gamma}/d\sqrt{\tau}$  and of the polarization factor  $\langle\xi_2\xi'_2\rangle$ , which may even become negative. As examples of such cases we give in Figs.4a,c the results for SM Higgs masses of  $m_H = 300\text{GeV}$  and  $m_H = 200\text{GeV}$  respectively; where [24] has again been used for calculating the needed Higgs total width. The corresponding sensitivities are indicated in the columns of Table 1 named after Fig.4a and Fig. 4c. As it is seen there, the sensitivity is quite considerable, in spite of the fact that the background contribution due to the  $(+-)$  photon-photon helicity amplitude which does not contain the Higgs effect, plays now a stronger role relatively to the  $(++)$  one. We also note that the smallness of the Higgs-width in these two cases, renders compelling the symmetric selection of  $ZZ$  invariant masses  $w_{\min}$  and  $w_{\max}$  around the value of  $m_H$ , with  $w_{\max} - w_{\min} < 20\text{GeV}$ ; see Table 1.

The sensitivity to Higgs masses like those used in Fig.4 can be further increased by reducing the energy  $\omega_0$  of the laser, while still keeping fixed the  $e^+e^-$  energy. This way, the value of  $x_0$  may be reduced so that the peak of the luminosity spectrum shown in Fig.2

Table 1: SM Higgs searches at a 0.5 TeV TESLA LC.  
(  $\mathcal{L}_{ee} = 300 \text{ fb}^{-1}/\text{year}$  )

	Fig. 3	Fig. 4a	Fig. 4b	Fig. 4c	Fig. 4d
$m_H$ (GeV)	400	300	300	200	200
$\Gamma_H$ (GeV)	28.89	8.51	8.51	1.428	1.428
$x_0 = x'_0$	4.83	4.83	2	4.83	1
$w_{\min}(GeV)$	340	290	290	195	195
$w_{\max}$ (GeV)	410	310	310	205	205
$\mathcal{N}^{\text{SM}}$	4635 (1381)	807 (240)	3637 (1083)	1033 (308)	4105 (1223)
$\mathcal{N}_{\text{Bg}}^{\text{SM}}$	3188 (950)	250 (75)	574 (171)	568 (169)	705 (210)
S.D.	25.6 (14)	35 (19)	128 (70)	19.5 (10.6)	128 (70)

coincides with  $\sqrt{\tau_H} \equiv m_H/\sqrt{s_{ee}}$ . Thus, choosing  $x_0 \simeq 1, 2$  for LC(500), sets the photon spectrum peak at  $\sqrt{\tau_H} \simeq 0.4, 0.6$  respectively, corresponding to  $m_H \simeq 200, 300$  GeV. The results are indicated in Figs.4b,d and the corresponding columns of Table 1. We see from them that the sensitivity indeed improves a lot. Tuning therefore the  $x_0, x'_0$ -values for such Higgs masses may be a very rewarding idea.

Before ending the discussion of SM masses in the 200-300 GeV region, we should also remark that if we insist in using  $x_0 = x'_0 = 4.83$  with LC(500) running at its top energy, then the employment of polarized beams as those indicated in Figs.2a,b is not particularly appropriate. The reason is that for such polarizations,  $\langle \xi_2 \xi'_2 \rangle$  is mostly negative at the relevant  $\sqrt{\tau_H}$  values. Therefore, the results of the columns labeled Fig.4a and Fig.4c in Table 1, could be improved by using instead unpolarized electron and laser photons, for which  $\langle \xi_2 \xi'_2 \rangle$  vanishes, and the relevant  $d\bar{L}_{\gamma\gamma}/d\sqrt{\tau}$  values are almost 20% larger; compare Fig.2c. Of course, these improvements would not be as large as those induced by the Fig.4b and Fig.4d choices in the same table<sup>5</sup>.

We next turn to the case of  $m_H = 500\text{GeV}$ , as an example of an SM Higgs mass which in the TESLA project can only be studied in the 800 GeV Linear Collider. For the machine luminosity in this case we use  $\mathcal{L}_{ee} = 500 \text{ fb}^{-1}/\text{year}$  at its top energy, while for lower energies the luminosity is scaled down linearly [23].

For the usual choice  $x_0 = x'_0 = 4.83$  with the  $e^\mp$  and laser polarizations indicated in Figs.2a,b, the results are shown in Fig.5a, where the dash line gives the prediction for  $m_H = 100\text{GeV}$  and serves as an estimate of the background. It is obvious from this figure, that in an LC(800) machine without some "tuning", it would not be possible to study

<sup>5</sup>These remarks are under the assumption that the distance between the production and interaction points of the backscattered photons is sufficiently small; see the second paper in [4].

such a high mass SM Higgs. This remains true, even if we had used instead unpolarized beams, as it can be inferred from the flux in Fig.2c, and the results in Fig.5a.

As a second attempt we assume  $x_0 = x'_0 = 2$  for the polarized beam case, which moves the peaks of the  $d\bar{L}_{\gamma\gamma}/d\sqrt{\tau}$  and  $\langle\xi_2\xi'_2\rangle$  distributions at  $\sqrt{s_{\gamma\gamma}} \simeq 500\text{GeV}$ , for LC(800) running at its top energy  $\sqrt{s_{ee}} = 0.8\text{TeV}$ ; compare Figs.2a,b. The corresponding results are given in Fig.5b. Using then (22, 23, 24) with  $w_{\min} = 0.43\text{TeV}$  and  $w_{\max} = 0.52\text{TeV}$ , we get  $\mathcal{N}^{\text{SM}} = 5562$  (1657),  $\mathcal{N}_{\text{Bg}}^{\text{SM}} = 5224$  (1556) for  $I_f = 0.47$  (0.14). The corresponding statistical significance of the effect is then determined by  $S.D. = 4.7$  (2.5).

This effect can be slightly increased by using instead  $x_0 = x'_0 = 4.83$  and tuning the energy of the LC(800), so that  $m_H/\sqrt{s_{ee}} \simeq 0.8$ ; *i.e.* at  $\sqrt{s_{ee}} = 0.63\text{ TeV}$ . The results so obtained are shown in Fig.5c. Using the same values for  $w_{\min}$  and  $w_{\max}$  and taking into account the fact that the LC(800) luminosity scales linearly as  $\sqrt{s_{ee}}$  decreases [23], we get  $\mathcal{N}^{\text{SM}} = 5731$  (1707),  $\mathcal{N}_{\text{Bg}}^{\text{SM}} = 5346$  (1592),  $S.D. = 5.3$  (2.9) for  $I_f = 0.47$  (0.14). It is worth remarking here that for such heavy and wide Higgs particles, tuning the LC energy is not much more efficient in improving the signal, than tuning the laser energies.

We should also remark here that the enhancements around the Higgs mass indicated in Figs.3,4,5 are not only due to the magnitude of the Higgs contribution sufficiently close to its mass shell, but also due to its constructive interference with the predominantly imaginary  $F_{++++}$  amplitude induced by the  $W$ -loop [9]. But as  $m_H$  increases, this interference decreases and eventually it becomes destructive. In fact, we have checked that exactly at  $w = m_H$ , the interference remains constructive only for Higgs masses  $\lesssim 460\text{ GeV}$ . Of course, off-shell there may be constructive interference even for higher Higgs masses. Because of this and the large SM Higgs width for sufficiently high masses, it seems possible to study through  $\gamma\gamma \rightarrow ZZ$  standard Higgs masses up to  $\simeq 500\text{GeV}$ ; compare Fig.5 and the above analysis .

Looking at the results presented above, we also note the fast fall-off of the sensitivity to SM Higgs particles, as the Higgs mass increases. This can be understood from the  $m_H$  dependence of the quantity  $Br(H \rightarrow \gamma\gamma)Br(H \rightarrow ZZ)/m_H^2$  controlling the size of the Higgs contribution; and from the rise of the  $\sigma(\gamma\gamma \rightarrow ZZ)_{\text{Laser}}$  background cross section with the energy; (compare [9]). For example,  $Br(H \rightarrow \gamma\gamma)Br(H \rightarrow ZZ)/m_H^2$  decreases by a factor of 80 as  $m_H$  increases from 300 to 500  $GeV$  (mainly due to the decrease of  $Br(H \rightarrow \gamma\gamma)$ ); while the background cross section increases by a factor 2 for the corresponding energy rise; compare *e.g.* [14, 4]. These two effects explain the strong decrease of the  $S.D.$  number as the Higgs mass increases.

### **SUSY cases:**

As an application to SUSY, we investigate models in which all soft SUSY breaking sfermion mass parameters are taken at the TeV scale and the stop mixing maximal [25]. Such models have the tendency to push the mass of the CP even  $h^0$  towards its highest possible values [24]. Thus, for a sufficiently heavy CP-odd  $A^0$  Higgs particle and a not very small  $\tan\beta$ , they should be well within the presently allowed region [1, 26, 27].

Assuming also the gaugino unification condition

$$M_1 = \frac{5}{3} \tan^2 \theta_W M_2 \quad ,$$

we present in the first three lines of Table 2 five Sets of values for the independent parameters  $\mu$ ,  $M_2$ ,  $M_{\tilde{f}}$ ,  $\tan \beta$  and  $A_t$ . Taking also the mass  $m_{A^0}$  of the CP-odd  $A^0$  as a further independent parameter, we show in the same table the implied stop, chargino and Higgs masses, as well as the Higgs widths and branching ratios calculated using HDECAY [24].

We have investigated  $\gamma\gamma \rightarrow H^0 \rightarrow ZZ$  cases where  $m_{A^0}$  is either 200 or 300 GeV, which imply similar (but somewhat higher masses) for the CP-even  $H^0$ . In all these cases, the  $H^0$  particle we wish to study, has a width of the order of 0.1 to 0.2 GeV.

Since this SUSY Higgs resonance is much narrower than the typical width of the peak of the photon-photon spectrum (about 10 GeV for  $\text{LC}(500)_{\gamma\gamma}$ ); the expected number of events within such a small region may be written as [2, 16, 5]

$$\mathcal{N}^{\text{SUSY}} \simeq I_f \mathcal{L}_{ee} \frac{1}{\sqrt{s_{ee}}} \left( \frac{d\bar{L}_{\gamma\gamma}}{d\sqrt{\tau}} \right)_{\tau=\tau_{H^0}} \cdot \left\{ \Sigma_0^{\text{SUSY}} + \langle \xi_2 \xi'_2 \rangle_{\tau=\tau_{H^0}} \cdot \Sigma_{22}^{\text{SUSY}} \right\} \quad , \quad (25)$$

$$\mathcal{N}_{\text{Bg}}^{\text{SUSY}} \simeq I_f \mathcal{L}_{ee} \frac{1}{\sqrt{s_{ee}}} \left( \frac{d\bar{L}_{\gamma\gamma}}{d\sqrt{\tau}} \right)_{\tau=\tau_{H^0}} \cdot \left\{ \Sigma_0^{\text{Bg}} + \langle \xi_2 \xi'_2 \rangle_{\tau=\tau_{H^0}} \cdot \Sigma_{22}^{\text{Bg}} \right\} \quad , \quad (26)$$

where

$$\Sigma_0^{\text{SUSY}} = \int_{m_{H^0}-5\text{GeV}}^{m_{H^0}+5\text{GeV}} dw \bar{\sigma}_0(\gamma\gamma \rightarrow ZZ) \quad , \quad (27)$$

$$\Sigma_{22}^{\text{SUSY}} = \int_{m_{H^0}-5\text{GeV}}^{m_{H^0}+5\text{GeV}} dw \bar{\sigma}_{22}(\gamma\gamma \rightarrow ZZ) \quad , \quad (28)$$

are expressed in terms of the  $\gamma\gamma \rightarrow ZZ$  subprocess cross sections defined in (17, 18). As before,  $\tau_{H^0} = m_{H^0}^2/s_{ee}$ . Notice that (25, 26), can immediately be derived from (22, 23) in the narrow width approximation.

As examples of the form of the  $\bar{\sigma}_0(\gamma\gamma \rightarrow ZZ)$  and  $\bar{\sigma}_{22}(\gamma\gamma \rightarrow ZZ)$  cross sections in the SUSY case, we show in Figs.6a,b the results for the parameter Sets 3 and 4 of Table 2. Quantities  $\Sigma_0^{\text{SUSY}}$  and  $\Sigma_{22}^{\text{SUSY}}$  are then directly calculated from them by integrating around the Higgs peak. The corresponding background quantities  $\Sigma_0^{\text{Bg}}$  and  $\Sigma_{22}^{\text{Bg}}$  are defined analogously to (27, 28) by subtracting the resonance contributions to the  $\bar{\sigma}_0$ ,  $\bar{\sigma}_{22}$  cross sections, which typically have the structure shown in Fig.6. The values of  $\Sigma_0^{\text{SUSY}}$ ,  $\Sigma_{22}^{\text{SUSY}}$ ,  $\Sigma_0^{\text{Bg}}$ ,  $\Sigma_{22}^{\text{Bg}}$  thus obtained, for the cases of the five SUSY Sets mentioned above, are indicated at the end of Table 2.

In analogy to (24), the  $H^0$ -sensitivities in the SUSY case are determined from (25, 26) and the results in Table 2, through

$$S.D. \equiv \frac{(\mathcal{N}^{\text{SUSY}} - \mathcal{N}_{\text{Bg}}^{\text{SUSY}})}{\sqrt{\mathcal{N}_{\text{Bg}}^{\text{SUSY}}}} \quad . \quad (29)$$

Table 2: SUSY Sets.  
(All running parameters are taken at the electroweak scale.)

	Set1	Set2	Set3	Set4	Set5
$M_2 = 200\text{GeV}$ , $\mu = 300\text{GeV}$ , $M_{\tilde{f}} = 1000\text{GeV}$					
$\tan\beta$	3		4		5
$A_t = A_b = A_\tau$ (GeV)	2550		2600		2550
$m_{\tilde{t}_1}$ (GeV)	785		777		781
$m_{\tilde{t}_2}$ (GeV)	1198		1204		1201
$m_{\tilde{\chi}_1}$ (GeV)	165		168		170
$m_{\tilde{\chi}_2}$ (GeV)	340		339		337
$m_{A^0}$ (GeV)	200	300	200	300	200
$m_{H^\pm}$ (GeV)	214	310	215	310	215
$m_{h^0}$	109	113	115	118	119
$m_{H^0}$ (GeV)	212	307	207	304	205
$\Gamma_{H^0}$ (GeV)	0.105	0.240	0.112	0.234	0.135
$Br(H^0 \rightarrow ZZ)$	0.188	0.069	0.123	0.0475	0.0747
$Br(H^0 \rightarrow \gamma\gamma) \times 10^5$	1.61	1.47	1.17	1.12	0.769
$\Sigma_0^{\text{SUSY}}$ (fb TeV)	0.99	0.64	0.64	0.58	0.39
$\Sigma_{22}^{\text{SUSY}}$ (fb TeV)	0.67	0.20	0.334	0.14	0.09
$\Sigma_0^{\text{Bg}}$ (fb TeV)	0.194	0.56	0.178	0.55	0.17
$\Sigma_{22}^{\text{Bg}}$ (fb TeV)	-0.122	0.11	-0.125	0.11	-0.124
	Set1	Set2	Set3	Set4	Set5

These sensitivities depend of course also on the LC luminosity and the parameters

$$\left(\frac{d\bar{L}_{\gamma\gamma}}{d\sqrt{\tau}}\right)_{\tau=\tau_{H^0}}, \quad \langle \xi_2 \xi_2' \rangle_{\tau=\tau_{H^0}},$$

which in turn are determined by the LC-energy and the  $x_0$ ,  $x'_0$  values and polarizations used. For definiteness we assume a TESLA LC(500), with a  $\mathcal{L}_{ee} = 300\text{fb}^{-1}/\text{year}$ , at the top of its energy [23]. We then discuss below the sensitivities for each of the five Sets of parameters in Table 2, by considering in each case, four different choices of the machine parameters. In the first three choices we use the electron and laser polarizations appearing in Figs.2a,b; while in the fourth choice, the unpolarized beams inducing the solid line prediction in Fig.2c are used. We first list the results for the four choices concerning Set 1, in which  $m_{H^0} \simeq 212$  GeV and  $\tan\beta = 3$ . They are

- Set 1, Choice 1. LC(500) is run at  $\sqrt{s_{ee}} = 0.5\text{TeV}$  using  $x_0 = x'_0 = 4.83$ . The electrons (positrons) and the laser photons are taken polarized with polarizations  $P_e = P'_e = 0.8$ ,  $P_\gamma = P'_\gamma = -1$ . For the  $m_{H^0}$ -value of Set 1, we then find  $\sqrt{\tau_{H^0}} = 0.42$ ,

implying from Fig.2a,b

$$\left(\frac{d\bar{L}_{\gamma\gamma}}{d\sqrt{\tau}}\right)_{\tau=\tau_{H^0}} = 1.25 \quad , \quad \langle \xi_2 \xi'_2 \rangle_{\tau=\tau_{H^0}} = -0.52 \quad ,$$

which through (25, 26 29) gives

$$\mathcal{N}^{\text{SUSY}} = 226 \text{ (67.4)} \quad , \quad \mathcal{N}_{\text{Bg}}^{\text{SUSY}} = 91 \text{ (27)} \quad , \quad S.D. = 14.2 \text{ (7.8)}$$

for  $I_f = 0.47$  (0.14) respectively.

- Set 1, Choice 2. LC(500) still runs at  $\sqrt{s_{ee}} = 0.5\text{TeV}$ , but  $x_0 = x'_0 = 1$  is now used, which for the  $m_{H^0}$ -value of Set 1 again gives  $\sqrt{\tau_{H^0}} = 0.42$ , implying from Fig.2a,b

$$\left(\frac{d\bar{L}_{\gamma\gamma}}{d\sqrt{\tau}}\right)_{\tau=\tau_{H^0}} = 1.89 \quad , \quad \langle \xi_2 \xi'_2 \rangle_{\tau=\tau_{H^0}} = 0.70 \quad .$$

Through (25, 26 29), this gives

$$\mathcal{N}^{\text{SUSY}} = 778 \text{ (232)} \quad , \quad \mathcal{N}_{\text{Bg}}^{\text{SUSY}} = 57.9 \text{ (17.2)} \quad , \quad S.D. = 94 \text{ (51)}$$

for  $I_f = 0.47$  (0.14) respectively.

- Set1, Choice 3. This is the "extreme tuning" case in which  $x_0 = x'_0 = 4.83$  is used, and LC(500) is tuned at  $\sqrt{s_{ee}} = 0.265 \text{ TeV}$ , so that for the  $m_{H^0}$ -value of Set 1 we are guaranteed to have  $\sqrt{\tau_{H^0}} \simeq 0.8$ , implying from Fig.2a,b

$$\left(\frac{d\bar{L}_{\gamma\gamma}}{d\sqrt{\tau}}\right)_{\tau=\tau_{H^0}} = 2 \quad , \quad \langle \xi_2 \xi'_2 \rangle_{\tau=\tau_{H^0}} = 0.92 \quad .$$

Through (25, 26 29) we then get

$$\mathcal{N}^{\text{SUSY}} = 906 \text{ (270)} \quad , \quad \mathcal{N}_{\text{Bg}}^{\text{SUSY}} = 46.1 \text{ (13.7)} \quad , \quad S.D. = 127 \text{ (69)}$$

for  $I_f = 0.47$  (0.14) respectively.

- Set 1, Choice 4. LC(500) now runs again at  $\sqrt{s_{ee}} = 0.5\text{TeV}$ , with  $x_0 = x'_0 = 4.83$ , but unpolarized electron and laser beams are used. Thus for the  $m_{H^0}$ -value of Set 1 implying  $\sqrt{\tau_{H^0}} = 0.42$ , we get from Fig.2c

$$\left(\frac{d\bar{L}_{\gamma\gamma}}{d\sqrt{\tau}}\right)_{\tau=\tau_{H^0}} = 1.49 \quad , \quad \langle \xi_2 \xi'_2 \rangle_{\tau=\tau_{H^0}} = 0 \quad .$$

Through (25, 26 29), this gives

$$\mathcal{N}^{\text{SUSY}} = 415 \text{ (124)} \quad , \quad \mathcal{N}_{\text{Bg}}^{\text{SUSY}} = 81.5 \text{ (24.3)} \quad , \quad S.D. = 79 \text{ (20)}$$

for  $I_f = 0.47$  (0.14) respectively.

Making a similar treatment for the cases of the other SUSY Sets of Table 2, we obtain for Sets 3 and 5 concerning an  $H^0$  in the mass region of 200 GeV, the results in Table 3; while in Table 4 we give the results for Sets 2 and 4 concerning  $m_{H^0} \sim 300$  GeV. As expected from the SM discussion about the 200-300 GeV mass region, the sensitivities in the case of Choice 4 (employing unpolarized beams) are always better than those of Choice 1, but worse than those of Choices 2 and 3.

Table 3: SUSY Sets 3 and 5 at LC(500),  
(Cases with  $m_{H^0} \sim 200$  GeV for  $I_f = 0.47$  (0.14).)

	Set 3				Set 5			
$\tan \beta$	4				5			
Choice	1	2	3	4	1	2	3	4
$\sqrt{s_{ee}}$ (TeV)	0.5	0.5	0.259	0.5	0.5	0.5	0.256	0.5
$x_0 = x'_0$	4.83	1	4.83	4.83	4.83	1	4.83	4.83
$\sqrt{\tau_{H^0}}$	0.414	0.414	0.8	0.414	0.41	0.41	0.8	0.41
$\left(\frac{d\bar{L}_{\gamma\gamma}}{d\sqrt{\tau}}\right)_{\tau_{H^0}}$	1.25	1.89	2	1.49	1.26	1.86	2	1.49
$\langle \xi_2 \xi'_2 \rangle_{\tau_{H^0}}$	-0.51	0.68	0.92	0	-0.5	0.6	0.92	0
$\mathcal{N}^{\text{SUSY}}$	165 (49)	462 (138)	534 (159)	269 (80.1)	122 (36.2)	233 (69.4)	267 (79.4)	164 (48.8)
$\mathcal{N}^{\text{SUSY}}_{\text{Bg}}$	85 (25)	66 (15)	36 (11)	75 (22.3)	81.4 (24.3)	49.6 (14.8)	31 (9.2)	71 (21.1)
S.D.	8.7 (4.8)	49 (32)	84 (45)	22 (12)	4.5 (2.4)	26 (14)	42 (23)	11 (6)

As we see from Tables 2-4, the number of standard deviations S.D. of the signal is largest in the lower side of  $\tan \beta$  and  $A^0$  (or  $H^0$ ) masses considered (*i.e.* for  $\tan \beta \simeq 3$  and  $m_{A^0} \simeq 200$  GeV). But as either  $\tan \beta$  or  $m_{A^0}$  increase, S.D. is diminishing rather quickly. For  $m_{A^0} = 200$  GeV, it is still sizable even for  $\tan \beta = 5$ , provided we tune the  $x_0$ ,  $x'_0$ -values at least.

For higher  $H^0$  masses, the situation becomes more difficult. Thus the sensitivity to  $m_{H^0} \sim 300$  GeV of an LC(500) TESLA machine can only reach some modest levels, provided that  $\tan \beta \lesssim 3$  and that  $x_0$ ,  $x'_0$  or energy tuning are applied; Compare the results in Tables 2 and 4.

We also note that while for  $m_{H^0} \sim 200$  GeV, LC-energy tuning seems to be more efficient than  $x_0$ ,  $x'_0$  tuning for improving the signal; they become comparable for  $m_{H^0} \sim 300$  GeV.

In order to understand the dependence in the Higgs mass of the observability of the above SUSY cases, one should not only consider, as in the SM case, the quantity  $Br(H \rightarrow \gamma\gamma)Br(H \rightarrow ZZ)/m_H^2$  and the energy rise of the background cross sections  $\sigma_0(\gamma\gamma \rightarrow ZZ)$

Table 4: SUSY Sets 2 and 4 at LC(500),  
(Cases with  $m_{H^0} \sim 300$  GeV for  $I_f = 0.47$  (0.14) ).

	Set 2				Set 4			
$\tan \beta$	3				4			
Choice	1	2	3	4	1	2	3	4
$\sqrt{s_{ee}}$ (TeV)	0.5	0.5	0.384	0.5	0.5	0.5	0.38	0.5
$x_0 = x'_0$	4.83	2	4.83	4.83	4.83	2	4.83	4.83
$\sqrt{\tau_{H^0}}$	0.613	0.613	0.8	0.613	0.608	0.608	0.8	0.613
$\left(\frac{d\mathcal{L}_{\gamma\gamma}}{d\sqrt{\tau}}\right)_{\tau_{H^0}}$	1.09	1.73	2	1.29	1.09	1.74	2	1.29
$\langle \xi_2 \xi'_2 \rangle_{\tau_{H^0}}$	-0.4	0.88	0.92	0	-0.4	0.85	0.92	0
$\mathcal{N}^{\text{SUSY}}$	173 (51.6)	398 (119)	465 (138)	231 (68.6)	162 (48.2)	341 (102)	398 (118)	211 (62.7)
$\mathcal{N}_{\text{Bg}}^{\text{SUSY}}$	159 (47.5)	320 (95.4)	373 (111)	202 (60.2)	156 (46.6)	315 (94)	367 (109)	200 (59.7)
S.D.	1.1 (0.6)	4.3 (2.4)	4.7 (2.6)	2.0 (1.1)	0.41 (0.23)	1.4 (0.79)	1.6 (0.87)	0.7 (0.4)

and  $\sigma_{22}(\gamma\gamma \rightarrow ZZ)$ ; but also the fact that the  $H^0$  is narrow, its width being much smaller than the width of the peak of the photon-photon spectrum ( $\Delta \simeq 10$  GeV). This last effect leads to a reduction of the signal by a factor ( $\Gamma_{H^0}/\Delta$ ); (in the SM case this effect does not occur for  $m_H \gtrsim 300$  GeV, because  $\Gamma_H \gtrsim 10$  GeV). Using then the  $\Gamma_H$  results given in Table 2, one can easily understand the values of the corresponding S.D. numbers.

We next briefly comment on the interference pattern between the  $H^0$ -pole and the background contribution in the SUSY case. Such an effect would be evident in Fig.6b, which corresponds to  $m_{H^0} = 300$  GeV and  $\Gamma_{H^0} = 0.234$  GeV, provided that the energy resolution were perfect. But no interference pattern is obvious in the  $m_{H^0} = 200$  GeV case of Fig.6a. Of course, with an energy resolution of about 10 GeV (as we have assumed in our analysis, due to the peak of the photon-photon spectrum) it is not possible to observe interference patterns of the type of Fig.6b, by just averaging the data symmetrically around the Higgs mass. Nevertheless, it is important to remember that they might exist and to search for them by trying various ways of binning the experimental data. In fact it is true that selections might exist which could appreciably modify the number of signal events, (say *e.g.* by selecting events mainly on one side of the resonance we are searching for) and thus help revealing a Higgs effect.

## 4 Conclusions

Assuming that the  $\gamma\gamma$  Collider will be realized some day by applying the laser backscattering idea to an  $e^+e^-$  or  $e^-e^-$  LC, we have studied the observability of a standard or SUSY heavy neutral Higgs boson produced in the  $s$ -channel through  $\gamma\gamma \rightarrow H^0 \rightarrow ZZ$ . One of the motivations for performing this work was to investigate whether we could exploit the striking predominance of the helicity conserving purely imaginary amplitudes expected for the background  $\gamma\gamma \rightarrow ZZ$  process at sufficiently high energies.

We have considered both, the case of the SM Higgs boson, as well as cases for the heavier CP-even  $H^0$  Higgs predicted in MSSM. Under such circumstances, we have computed the amplitude for  $\gamma\gamma \rightarrow H^0 \rightarrow ZZ$  in which the  $\gamma\gamma \rightarrow H^0$  coupling arises at one-loop, while  $H^0 \rightarrow ZZ$  exists at tree level; as well as the background  $\gamma\gamma \rightarrow ZZ$  contribution arising through one-loop box amplitudes. In Section 2 and the Appendix, we have collected the explicit analytic expressions for the Higgs-pole and background amplitudes in the SM and the MSSM cases. They are presented in terms of Passarino-Veltman functions immediately suitable for computation. For most of the formulae we refer to [7, 8, 9], except for the mixed chargino box contributions arising from two different charginos running along the box diagram, which appear here for the first time.

We have then studied the interplay of the resonant Higgs contribution with the predominantly helicity conserving imaginary background amplitude at sufficiently high energy. Depending on the parameters of the model, remarkable interference effects may appear, which in some cases enhance the Higgs signal.

Our first application has been to the standard Higgs search. For LC(500), using the photon-photon spectrum implied by the highest meaningful laser energy ( $x_0 = 4.83$ ) with circular photon polarizations and longitudinally polarized  $e^\pm$  beams, we have shown what would be the signal of an SM Higgs boson of arbitrary mass, above the  $ZZ$ -threshold. In these illustrations we have assumed the machine to be running at its top energy of 0.5 TeV.

Provided the Higgs mass is known, it should also be possible to optimize the signal; either by changing the energy of the laser for fixed  $e^+e^-$  energy, or by tuning the LC energy. We have made illustrations for  $m_H = 200, 300, 400$  GeV at LC(500) and for  $m_H = 500$  GeV at LC(800), using the TESLA luminosities.

We find that for masses in the region ( $m_H \simeq 200 - 300$  GeV), the narrow Higgs peak largely dominates the background, and the interference effect does not play an important role; compare Fig.4. For such Higgs masses, we have also observed that when running LC(500) at its top energy, the relevant values of  $\langle \xi_2 \xi'_2 \rangle$  are largely negative, thus reducing the signal. Thus, under such energy running conditions and Higgs masses, the use of unpolarized electron and laser beams will be more efficient than the use of the polarized beams mentioned above. Of course, when  $x_0$ ,  $x'_0$  or energy tuning is employed, the importance of polarizations is re-established.

For higher masses (400 – 450 GeV), the constructive interference between the large imaginary parts of the Higgs and of the background amplitudes, increases the size of the

Higgs contribution. This is stronger in the region just below the Higgs peak (compare Fig.3), and it appears even for higher masses (see Fig.5b,c). In such cases, the interference pattern plays an important role for the Higgs detection.

Therefore, the measurement of the various terms of the polarized cross section  $\bar{\sigma}_j(\gamma\gamma \rightarrow ZZ)$ , constitutes a useful tool of the standard Higgs search, for Higgs masses in the range ( $2m_Z \lesssim m_H \lesssim 500$  GeV). Compare the results in Table 1; and those for  $m_H \simeq 500$  GeV at LC(800), provided that either laser energy or the LC energy is appropriately tuned.

For even higher Higgs masses though, the strongly decreasing  $Br(H \rightarrow \gamma\gamma)$  branching ratio prohibits an observable effect.

We have then turned to SUSY and considered the effects of the heavier CP-even  $H^0$  predicted in MSSM. The search has been concentrated on the part of the MSSM parameter space in which all sfermion SUSY breaking masses and their mixing are sufficiently large, in order to guarantee that  $m_{h^0}$  is well within the presently allowed region. We have considered five such Sets of SUSY parameters leading to  $m_{H^0}$  in either the 200GeV or the 300GeV mass region; compare Table 2. In all such cases, the SUSY  $H^0$  boson differs from the SM one, by having a much narrower width and a smaller branching ratio to  $ZZ$ .

For the observability of the  $H^0$  predicted in each of the above parameter Sets, we have studied, four choices of LC running conditions; compare Tables 3 and 4. In the first three choices, polarized  $e^\mp$  and laser beams are used with polarizations  $P_e = P'_e = 0.8$  and  $P_\gamma = P'_\gamma = -1$  respectively; while in the fourth choice fully unpolarized beams were employed. As in the SM case, we have found, that when running LC(500) at its top energy with  $x_0 = 4.83$ , the use of unpolarized beams for studying Higgs masses in the 200-300GeV region is more advantageous, than the use of the aforementioned polarizations. But, the importance of polarization is re-established when either  $x_0$ ,  $x'_0$  or energy tuning is employed in order to improve the signal.

Our overall conclusion is that the observability limit in SUSY decreases to about  $m_{H^0} \sim 300$  GeV for  $\tan\beta \lesssim 4$ ; while for  $\tan\beta \simeq 5$  it goes down to almost 200 GeV; see Tables 2-4. In the computations we have of course taken into account the SUSY box contributions to  $\gamma\gamma \rightarrow ZZ$  background.

We should also remark on the basis of the various numerical investigations performed, that the interference pattern between the Higgs-pole and background contributions varies, depending on the values of the SUSY parameters used. Examples of such an effect may be seen in Figs.6a,b. This is similar to what has also been observed in the SM case above. For comparison, in all SM cases we have also given the results for  $m_H = 100$  GeV.

In conclusion we can say that an experimental investigation of the  $\gamma\gamma \rightarrow ZZ$  process and an analysis taking into account the interference between the Higgs resonance and the one loop background amplitudes, should be helpful for the identification of a scalar Higgs-like candidate.

### Acknowledgments.

We are pleased to thank Abdelhak Djouadi for very useful and informative discussions

about the SUSY Higgs properties. One of us (GJG) would also like to thank the CERN Theory Division for the hospitality extended to him while part of this work was performed.

## Appendix: The $\gamma\gamma \rightarrow ZZ$ amplitudes in the Standard and SUSY models.

The invariant helicity amplitudes for the process

$$\gamma(p_1, \lambda_1)\gamma(p_2, \lambda_2) \rightarrow Z(p_3, \lambda_3)Z(p_4, \lambda_4) \quad , \quad (\text{A.1})$$

are denoted as<sup>6</sup>  $F_{\lambda_1\lambda_2\lambda_3\lambda_4}(\beta_Z, \hat{t}, \hat{u})$ , where the momenta and helicities of the incoming photons and outgoing  $Z$ 's are indicated in parentheses, and

$$\hat{s} = (p_1 + p_2)^2 = \frac{4m_Z^2}{1 - \beta_Z^2} \quad , \quad \hat{t} = (p_1 - p_3)^2 \quad , \quad \hat{u} = (p_1 - p_4)^2 \quad , \quad (\text{A.2})$$

$$\hat{s}_4 = \hat{s} - 4m_Z^2 \quad , \quad \hat{s}_2 = \hat{s} - 2m_Z^2 \quad , \quad \hat{t}_1 = \hat{t} - m_Z^2 \quad , \quad \hat{u}_1 = \hat{u} - m_Z^2 \quad (\text{A.3})$$

are used. Denoting by  $\vartheta^*$  the c.m. scattering angle of  $\gamma\gamma \rightarrow ZZ$ , we also note

$$\hat{t} = m_Z^2 - \frac{\hat{s}}{2}(1 - \beta_Z \cos \vartheta^*) \quad , \quad \hat{u} = m_Z^2 - \frac{\hat{s}}{2}(1 + \beta_Z \cos \vartheta^*) \quad , \quad (\text{A.4})$$

$$Y = \hat{t}\hat{u} - m_Z^4 = \frac{s^2\beta_Z^2}{4}\sin^2 \vartheta^* = \hat{s}p_{TZ}^2 \quad , \quad \Delta = \sqrt{\frac{\hat{s}m_Z^2}{2Y}} \quad , \quad (\text{A.5})$$

where  $p_{TZ}$  is the  $Z$  transverse momentum.

The parameter  $\beta_Z$  in (A.2) coincides with the  $Z$ -velocity in the  $ZZ$  c.m. frame. As in [8, 7, 9] it is used instead of  $\hat{s}$ . The standard form of the  $Z$  polarization vectors implies the useful relation

$$F_{\lambda_1\lambda_2\lambda_3\lambda_4}(\beta_Z, \hat{t}, \hat{u}) = F_{\lambda_1\lambda_2, -\lambda_3, -\lambda_4}(-\beta_Z, \hat{t}, \hat{u})(-1)^{\lambda_3 - \lambda_4} \quad , \quad (\text{A.6})$$

among the various helicity amplitudes. In addition, Bose statistics, combined with the Jacob-Wick (JW) [28] phase conventions demands

$$F_{\lambda_1\lambda_2\lambda_3\lambda_4}(\beta_Z, \hat{t}, \hat{u}) = F_{\lambda_2\lambda_1\lambda_4\lambda_3}(\beta_Z, \hat{t}, \hat{u})(-1)^{\lambda_3 - \lambda_4} \quad , \quad (\text{A.7})$$

$$F_{\lambda_1\lambda_2\lambda_3\lambda_4}(\beta_Z, \hat{t}, \hat{u}) = F_{\lambda_2\lambda_1\lambda_3\lambda_4}(\beta_Z, \hat{u}, \hat{t})(-1)^{\lambda_3 - \lambda_4} \quad , \quad (\text{A.8})$$

$$F_{\lambda_1\lambda_2\lambda_3\lambda_4}(\beta_Z, \hat{t}, \hat{u}) = F_{\lambda_1\lambda_2\lambda_4\lambda_3}(\beta_Z, \hat{u}, \hat{t}) \quad . \quad (\text{A.9})$$

while CP invariance, being equivalent to parity invariance at the 1-loop level, implies<sup>7</sup>

$$F_{\lambda_1\lambda_2\lambda_3\lambda_4}(\beta_Z, \hat{t}, \hat{u}) = F_{-\lambda_1, -\lambda_2, -\lambda_3, -\lambda_4}(\beta_Z, \hat{t}, \hat{u})(-1)^{\lambda_3 - \lambda_4} \quad . \quad (\text{A.10})$$

Using (A.6) we remark that

$$F_{++--}(\beta_Z, \hat{t}, \hat{u}) = F_{++++}(-\beta_Z, \hat{t}, \hat{u}) \quad , \quad (\text{A.11})$$

$$F_{++-0}(\beta_Z, \hat{t}, \hat{u}) = -F_{+++0}(-\beta_Z, \hat{t}, \hat{u}) \quad , \quad (\text{A.12})$$

---

<sup>6</sup>The same definitions as in [9] are used.

<sup>7</sup>A sign error in Eqs.(A.13) of [9] is corrected in (A.12) here.

which combined with ( $\hat{t} \leftrightarrow \hat{u}$ ) or helicity changes and the use of (A.7-A.10), allow to express the 36  $\gamma\gamma \rightarrow ZZ$  helicity amplitudes in terms of just the eight independent ones [9, 8, 7]

$$\begin{aligned} & F_{++++}(\beta_Z, \hat{t}, \hat{u}) , \quad F_{++++}(\beta_Z, \hat{t}, \hat{u}) , \quad F_{+--+}(\beta_Z, \hat{t}, \hat{u}) , \quad F_{+-00}(\beta_Z, \hat{t}, \hat{u}) , \\ & F_{++00}(\beta_Z, \hat{t}, \hat{u}) , \quad F_{++++}(\beta_Z, \hat{t}, \hat{u}) , \quad F_{+-+0}(\beta_Z, \hat{t}, \hat{u}) , \quad F_{+--+}(\beta_Z, \hat{t}, \hat{u}) . \end{aligned} \quad (\text{A.13})$$

In the non-linear gauge of [17] that we are using here, there are only two types of contributions to these amplitudes, in either the SM or SUSY models; see Fig.1. The first consists of the one-particle irreducible one-loop diagrams involving four external legs, similar to those contributing to the  $\gamma\gamma \rightarrow \gamma\gamma$  and  $\gamma\gamma \rightarrow \gamma Z$  processes [11, 12, 8]. We depict the generic form of these diagrams in Fig.1a and call them "boxes". Their contributions are given in this Appendix. The second type (discussed in Section 2) are one-particle reducible diagrams containing a Higgs s-channel pole and involving an<sup>8</sup>  $h^0\gamma\gamma$  vertex subdiagram [8]; see Fig1b.

### The scalar boxes.

Such contributions are generated in MSSM through the effective Lagrangian

$$\mathcal{L}_{V\bar{S}S} = -ie(Q_S A^\mu + g_S^Z Z^\mu)(S^* \overleftrightarrow{\partial}_\mu S) + e^2(Q_S A^\mu + g_S^Z Z^\mu)^2 |S|^2 , \quad (\text{A.14})$$

where  $S$  is any scalar field. In the minimal SUSY case where  $S = \tilde{t}_L, \tilde{t}_R, \tilde{b}_L, \tilde{b}_R, \tilde{\tau}_L, \tilde{\tau}_R, \tilde{\nu}_L$ , or <sup>9</sup>  $H^+$ , the corresponding coupling is

$$g_S^Z = \frac{1}{s_W c_W} (t_3^S - Q_S s_W^2) , \quad (\text{A.15})$$

in which  $t_3^S$  denotes the third isospin component of  $S$ .

The contribution to  $\gamma\gamma \rightarrow ZZ$  of any such scalar particle is [9]

$$F_{\lambda_1 \lambda_2 \lambda_3 \lambda_4}^S(\beta_Z, \hat{t}, \hat{u}) \equiv \alpha^2 Q_S^2 N_S^c (g_S^Z)^2 A_{\lambda_1 \lambda_2 \lambda_3 \lambda_4}^S(\beta_Z, \hat{t}, \hat{u}; m) , \quad (\text{A.16})$$

where  $N_S^c$  counts the colour multiplicity of  $S$ , and  $A_{\lambda_1 \lambda_2 \lambda_3 \lambda_4}^S$  is given by (A.34-A.41) in [9].

In cases like  $\tilde{t}_{1,2}$ , the non-diagonal mass matrix

$$\begin{pmatrix} \tilde{t}_L \\ \tilde{t}_R \end{pmatrix} = \begin{pmatrix} \cos \theta_t & -\sin \theta_t \text{Sign}(A_t - \mu \cot \beta) \\ \sin \theta_t \text{Sign}(A_t - \mu \cot \beta) & \cos \theta_t \end{pmatrix} \begin{pmatrix} \tilde{t}_1 \\ \tilde{t}_2 \end{pmatrix} , \quad (\text{A.17})$$

implies that the mixing angle always satisfies

$$\frac{\pi}{2} < \theta_t < \pi , \quad (\text{A.18})$$

---

<sup>8</sup>Here  $h^0$  denotes any neutral Higgs boson.

<sup>9</sup>For  $H^+$  we have  $t_3^{H^+} = 1/2$  and  $Q_{H^+} = 1$ .

and it is fully determined by

$$\sin(2\theta_t) = \frac{2m_t|A_t - \mu \cot \beta|}{m_{\tilde{t}_1}^2 - m_{\tilde{t}_2}^2} \quad , \quad (\text{A.19})$$

provided we define  $m_{\tilde{t}_1} < m_{\tilde{t}_2}$ , and  $A_t$  is real.

Then, the single  $\tilde{t}_1$ -box contribution is given by (A.16) for

$$g_{\tilde{t}_1}^Z = \frac{1}{s_W c_W} \left[ \frac{1}{2} \cos^2 \theta_t - \frac{2s_W^2}{3} \right] \quad , \quad (\text{A.20})$$

while for the single  $\tilde{t}_2$  one

$$g_{\tilde{t}_2}^Z = \frac{1}{s_W c_W} \left[ \frac{1}{2} \sin^2 \theta_t - \frac{2s_W^2}{3} \right] \quad (\text{A.21})$$

should be used. In principle, we should also consider the mixed box contribution arising when both  $\tilde{t}_1$  and  $\tilde{t}_2$  are running along the box sides. Since such mixed contributions are expected to be at most of similar magnitude to the one coming from the single  $\tilde{t}_1$ -box [29], which is already known to be extremely small [9], we have not calculated them.

If  $\tan \beta \gtrsim 10$ , then the  $\tilde{b}_1$ -squark or  $\tilde{\tau}_1$ -slepton contributions may be of similar magnitude. If desired, they may be directly obtained from (A.16) using the appropriate mixing matrix. Since in the numerical examples we consider these (as well as  $\tilde{t}_2$ ) are very heavy, we refrain from giving their explicit contributions.

### The $W$ -boxes.

These are 1-loop diagrams involving four external legs, with a  $W$ , Goldstone or FP-ghost running along the loop. They have first been presented by [8]. We write them as

$$F_{\lambda_1 \lambda_2 \lambda_3 \lambda_4}^W(\beta_Z, \hat{t}, \hat{u}) \equiv \frac{\alpha^2}{s_W^2} A_{\lambda_1 \lambda_2 \lambda_3 \lambda_4}^W(\beta_Z, \hat{t}, \hat{u}) \quad , \quad (\text{A.22})$$

with  $A_{\lambda_1 \lambda_2 \lambda_3 \lambda_4}^W$  given in (A.42-A.51) of [9].

### The fermion boxes.

If the effective  $(\gamma, Z)f\bar{f}$  interaction is written as

$$\mathcal{L}_{Vff} = -eQ_f A^\mu \bar{f} \gamma_\mu f - eZ^\mu \bar{f} (\gamma_\mu g_{vf}^Z - \gamma_\mu \gamma_5 g_{af}^Z) f \quad , \quad (\text{A.23})$$

then the fermion loop contribution to the  $\gamma\gamma \rightarrow ZZ$  helicity amplitude for a fermion of mass  $m_f$ , is given by [7, 9]

$$F_{\lambda_1 \lambda_2 \lambda_3 \lambda_4}^f(\beta_Z, \hat{t}, \hat{u}) \equiv \alpha^2 Q_f^2 N_f^c \left\{ (g_{vf}^Z)^2 A_{\lambda_1 \lambda_2 \lambda_3 \lambda_4}^{vf}(\beta_Z, \hat{t}, \hat{u}; m_f) + (g_{af}^Z)^2 A_{\lambda_1 \lambda_2 \lambda_3 \lambda_4}^{af}(\beta_Z, \hat{t}, \hat{u}; m_f) \right\} \quad , \quad (\text{A.24})$$

where  $N_f^c$  counts the colour multiplicity and  $A^{vf}$ ,  $A^{af}$  are given by (A.55-A.71) of [9].

For quarks and leptons

$$g_{vf}^Z = \frac{t_3^f - 2Q_f s_W^2}{2s_W c_W} \quad , \quad g_{af}^Z = \frac{t_3^f}{2s_W c_W} \quad , \quad (\text{A.25})$$

where  $t_3^f$  is the third isospin component of the fermion, and  $Q_f$  is its charge.

The specific case of a chargino fermion requires a more extensive discussion, because of their possible mixed coupling to  $Z$ . The relevant parameters are determined by the mass matrix

$$\mathcal{L}_{M_\chi} = -(\tilde{W}^{-\tau}, \tilde{H}_1^{-\tau})_L \cdot C \cdot \begin{pmatrix} M_2 & \sqrt{2}m_W \sin \beta \\ \sqrt{2}m_W \cos \beta & +\mu \end{pmatrix} \begin{pmatrix} \tilde{W}^+ \\ \tilde{H}_2^+ \end{pmatrix}_L + \text{h.c.} \quad , \quad (\text{A.26})$$

leading to the physical chargino masses

$$m_{\tilde{\chi}_1, \tilde{\chi}_2} = \frac{1}{\sqrt{2}}[M_2^2 + \mu^2 + 2m_W^2 \mp \tilde{D}]^{1/2} \quad , \quad (\text{A.27})$$

where

$$\tilde{D} \equiv [(M_2^2 + \mu^2 + 2m_W^2)^2 - 4(M_2\mu - m_W^2 \sin(2\beta))^2]^{1/2} \quad , \quad (\text{A.28})$$

for any sign of  $M_2$ ,  $\mu$ . Defining then the mixing-angles  $\phi_R, \phi_L$  as [30]

$$\begin{aligned} \cos \phi_L &= -\frac{1}{\sqrt{2\tilde{D}}}[\tilde{D} - M_2^2 + \mu^2 + 2m_W^2 \cos 2\beta]^{1/2} \quad , \\ \cos \phi_R &= -\frac{1}{\sqrt{2\tilde{D}}}[\tilde{D} - M_2^2 + \mu^2 - 2m_W^2 \cos 2\beta]^{1/2} \quad , \end{aligned} \quad (\text{A.29})$$

so that they always lie in the second quarter

$$\frac{\pi}{2} \leq \phi_L < \pi \quad , \quad \frac{\pi}{2} \leq \phi_R < \pi \quad ; \quad (\text{A.30})$$

the effective Lagrangian for the  $(\gamma, Z)$ -chargino interaction becomes<sup>10</sup>

$$\begin{aligned} \mathcal{L} &= -eA^\mu \bar{\tilde{\chi}}_j \gamma_\mu \tilde{\chi}_j - eZ^\mu \bar{\tilde{\chi}}_j (\gamma_\mu g_{vj} - \gamma_\mu \gamma_5 g_{aj}) \tilde{\chi}_j \\ &\quad - eZ^\mu [\bar{\tilde{\chi}}_1 (\gamma_\mu g_{v12} - \gamma_\mu \gamma_5 g_{a12}) \tilde{\chi}_2 + \text{h.c.}] \quad , \end{aligned} \quad (\text{A.31})$$

where

$$\begin{aligned} g_{v1} &= \frac{1}{2s_W c_W} \left( \frac{3}{2} - 2s_W^2 + \frac{1}{4}[\cos 2\phi_L + \cos 2\phi_R] \right) \quad , \\ g_{a1} &= -\frac{1}{8s_W c_W} [\cos 2\phi_L - \cos 2\phi_R] \quad , \end{aligned} \quad (\text{A.32})$$

---

<sup>10</sup>The chargino field is always defined so that it absorbs a positive chargino particle; *i.e.*  $\tilde{\chi}_j \equiv \tilde{\chi}_j^+$  ( $j = 1, 2$ ).

$$\begin{aligned}
g_{v2} &= \frac{1}{2s_W c_W} \left( \frac{3}{2} - 2s_W^2 - \frac{1}{4} [\cos 2\phi_L + \cos 2\phi_R] \right) , \\
g_{a2} &= \frac{1}{8s_W c_W} [\cos 2\phi_L - \cos 2\phi_R] , 
\end{aligned} \tag{A.33}$$

$$\begin{aligned}
g_{v12} &= - \frac{\text{Sign}(M_2)}{8s_W c_W} [\tilde{\mathcal{B}}_R \tilde{\Delta}_{12} \sin 2\phi_R + \tilde{\mathcal{B}}_L \sin 2\phi_L] , \\
g_{a12} &= - \frac{\text{Sign}(M_2)}{8s_W c_W} [\tilde{\mathcal{B}}_R \tilde{\Delta}_{12} \sin 2\phi_R - \tilde{\mathcal{B}}_L \sin 2\phi_L] . 
\end{aligned} \tag{A.34}$$

The box-contribution from the single chargino couplings in (A.32, A.33) are given by the same expressions (A.24). But for charginos we also have the "mixed"  $Z\tilde{\chi}_1\tilde{\chi}_2$ -couplings appearing in (A.34), which generate boxes with two different charginos running along the loop. These couplings, as well as those of the neutral Higgs to charginos defined in Section 2, depend on the sign-quantities

$$\begin{aligned}
\tilde{\mathcal{B}}_L &= \text{Sign}(\mu \sin \beta + M_2 \cos \beta) , \\
\tilde{\mathcal{B}}_R &= \text{Sign}(\mu \cos \beta + M_2 \sin \beta) , \\
\tilde{\mathcal{B}}_{LR} &\equiv \text{Sign} \left( M_2 \mu + \frac{\mu^2 + M_2^2}{2} \sin 2\beta \right) = \tilde{\mathcal{B}}_L \tilde{\mathcal{B}}_R , \\
\tilde{\Delta}_1 &= \text{Sign}(M_2 [\tilde{D} - M_2^2 + \mu^2 - 2m_W^2] - 2m_W^2 \mu \sin 2\beta) , \\
\tilde{\Delta}_2 &= \text{Sign}(\mu [\tilde{D} - M_2^2 + \mu^2 + 2m_W^2] + 2m_W^2 M_2 \sin 2\beta) , \\
\tilde{\Delta}_{12} &\equiv \text{Sign}(M_2 \mu - m_W^2 \sin 2\beta) = \tilde{\Delta}_1 \tilde{\Delta}_2 , 
\end{aligned} \tag{A.35}$$

constructed to guarantee the positivity of the physical chargino masses and the usual relation between the fields absorbing the positive and negative charginos; *i.e.*  $C\tilde{\chi}^{+\tau} = \tilde{\chi}^-$  [30].

### The mixed chargino boxes.

This contribution, generated by the  $Z\tilde{\chi}_1\tilde{\chi}_2$  - couplings in (A.34), is denoted as<sup>11</sup>

$$\begin{aligned}
F_{\lambda_1 \lambda_2 \lambda_3 \lambda_4}^{\tilde{\chi}_1 \tilde{\chi}_2}(\beta_Z, \hat{t}, \hat{u}) &\equiv \alpha^2 [(g_{v12})^2 + (g_{a12})^2] (-1)^{1-\lambda_4} A_{\lambda_1 \lambda_2 \lambda_3 \lambda_4}^{(\tilde{\chi}_1 \tilde{\chi}_2 1)}(\beta_Z, \hat{t}, \hat{u}; m_{\tilde{\chi}_1^2}, m_{\tilde{\chi}_2^2}) \\
&+ \alpha^2 [(g_{v12})^2 - (g_{a12})^2] m_{\tilde{\chi}_1} m_{\tilde{\chi}_2} (-1)^{1-\lambda_4} A_{\lambda_1 \lambda_2 \lambda_3 \lambda_4}^{(\tilde{\chi}_1 \tilde{\chi}_2 2)}(\beta_Z, \hat{t}, \hat{u}; m_{\tilde{\chi}_1^2}, m_{\tilde{\chi}_2^2}) . 
\end{aligned} \tag{A.36}$$

The form of (A.36) is motivated by the fact that the structure of the mixed boxes allow only the existence of either  $g_{v12}^2$  or  $g_{a12}^2$  terms, which are related to each other through the substitutions:

$$g_{v12} \leftrightarrow g_{a12} \quad \text{and} \quad (m_1, m_2) \leftrightarrow (-m_1, m_2) .$$

To describe this mixed chargino contribution, we need the Passarino-Veltman functions [18], for which we follow the notation of [19] and the abbreviations<sup>12</sup>

$$B_Z^{11}(\hat{s}) \equiv B_0(\hat{s}; m_1, m_1) - B_0(m_Z^2 + i\epsilon; m_1, m_2) , \tag{A.37}$$

<sup>11</sup>The factor  $(-1)^{1-\lambda_4}$  comes from the JW helicity convention [28].

<sup>12</sup>In the middle terms of (A.40-A.46)  $k_1 = p_1$ ,  $k_2 = p_2$  denote the momenta of the photons, while  $k_3 = -p_3$ ,  $k_4 = -p_4$  those of the  $A^0$ , always taken as incoming; compare (A.1).

$$B_Z^{22}(\hat{s}) \equiv B_0(\hat{s}; m_2, m_2) - B_0(m_Z^2 + i\epsilon; m_1, m_2) , \quad (\text{A.38})$$

$$B_Z^{12}(\hat{s}) \equiv B_0(\hat{s}; m_1, m_2) - B_0(m_Z^2 + i\epsilon; m_1, m_2) , \quad (\text{A.39})$$

$$C_0^{abc}(\hat{s}) \equiv C_0(k_1, k_2) = C_0(0, 0, \hat{s}; m_a, m_b, m_c) , \quad (\text{A.40})$$

$$C_Z^{abc}(\hat{u}) \equiv C_0(k_3, k_2) = C_0(m_Z^2, 0, \hat{u}; m_a, m_b, m_c) , \quad (\text{A.41})$$

$$C_{ZZ}^{abc}(\hat{s}) \equiv C_0(k_3, k_4) = C_0(m_Z^2, m_Z^2, \hat{s}; m_a, m_b, m_c) , \quad (\text{A.42})$$

$$D_{ZZ}^{abcd}(\hat{s}, \hat{t}) \equiv D_0(k_4, k_3, k_1) = D_0(m_Z^2, m_Z^2, 0, 0, \hat{s}, \hat{t}; m_a, m_b, m_c, m_d) , \quad (\text{A.43})$$

$$D_{ZZ}^{abcd}(\hat{s}, \hat{u}) \equiv D_0(k_3, k_4, k_1) = D_0(m_Z^2, m_Z^2, 0, 0, \hat{s}, \hat{u}; m_a, m_b, m_c, m_d) , \quad (\text{A.44})$$

$$D_{ZZ}^{abcd}(\hat{t}, \hat{u}) \equiv D_0(k_3, k_1, k_4) = D_0(m_Z^2, 0, m_Z^2, 0, \hat{t}, \hat{u}; m_a, m_b, m_c, m_d) , \quad (\text{A.45})$$

$$D_{ZZ}^{abcd}(\hat{u}, \hat{t}) \equiv D_0(k_4, k_1, k_3) = D_0(m_Z^2, 0, m_Z^2, 0, \hat{u}, \hat{t}; m_a, m_b, m_c, m_d) , \quad (\text{A.46})$$

$$\tilde{F}^{ab}(\hat{s}, \hat{t}, \hat{u}) = D_{ZZ}^{abba}(\hat{t}, \hat{u}) + D_{ZZ}^{abaa}(\hat{s}, \hat{t}) + D_{ZZ}^{abaa}(\hat{s}, \hat{u}) , \quad (\text{A.47})$$

$$E_1^{ab}(\hat{s}, \hat{u}) = 2\hat{u}_1 C_Z^{baa}(\hat{u}) - \hat{s}\hat{u} D_{ZZ}^{abaa}(\hat{s}, \hat{u}) , \quad (\text{A.48})$$

$$\begin{aligned} E_2^{ab}(\hat{t}, \hat{u}) &= \hat{t}_1 [C_Z^{abb}(\hat{t}) + C_Z^{baa}(\hat{t})] + \hat{u}_1 [C_Z^{abb}(\hat{u}) + C_Z^{baa}(\hat{u})] \\ &\quad - Y D_{ZZ}^{abba}(\hat{t}, \hat{u}) , \end{aligned} \quad (\text{A.49})$$

which are closely related to those in<sup>13</sup> Eqs.(A.14 - A.24) of [9].

We also note that

$$\begin{aligned} D_{ZZ}^{abba}(\hat{t}, \hat{u}) &= D_{ZZ}^{abba}(\hat{u}, \hat{t}) = D_{ZZ}^{baab}(\hat{t}, \hat{u}) = D_{ZZ}^{baab}(\hat{u}, \hat{t}) , \\ \tilde{F}^{ab}(\hat{s}, \hat{t}, \hat{u}) &= \tilde{F}^{ab}(\hat{s}, \hat{u}, \hat{t}) , \quad E_2^{ab}(\hat{t}, \hat{u}) = E_2^{ab}(\hat{u}, \hat{t}) = E_2^{ba}(\hat{t}, \hat{u}) . \end{aligned} \quad (\text{A.50})$$

Thus, the eight basic amplitudes listed in (A.13, A.36) are determined by<sup>14</sup>

$$\begin{aligned} A_{++++}^{(\tilde{\chi}_1 \tilde{\chi}_2^{11})}(\beta_Z, \hat{t}, \hat{u}; m_1^2, m_2^2) &= -\frac{16[m_Z^2(2Y - \hat{s}\hat{s}_4) + \beta_Z \hat{s}Y]}{\hat{s}_4 \hat{t}_1 \hat{u}_1} \\ &+ \frac{4(\hat{s}_2 + \hat{s}\beta_Z)}{\hat{s}_4 \hat{s}} \left[ \frac{(2Y - \hat{s}\hat{s}_4)}{\hat{s}} E_2^{12}(\hat{t}, \hat{u}) + \frac{4m_Z^2 Y + 2\hat{t}_1(2\hat{t}_1 + \hat{s})(\hat{t} + m_Z^2)}{\hat{t}_1^2} B_Z^{12}(\hat{t}) \right. \\ &\quad \left. + \frac{4m_Z^2 Y + 2\hat{u}_1(2\hat{u}_1 + \hat{s})(\hat{u} + m_Z^2)}{\hat{u}_1^2} B_Z^{12}(\hat{u}) \right] \\ &+ \frac{8}{\hat{s}_4} \left\{ -2m_1^2[2(m_Z^2 + m_2^2 - m_1^2) + \hat{s}\beta_Z] C_0^{111}(\hat{s}) + \frac{(m_1^2 - m_2^2)^2}{\hat{s}} [E_2^{12}(\hat{t}, \hat{u}) \right. \\ &\quad \left. - 2\hat{s}m_1^2 \tilde{F}^{12}(\hat{s}, \hat{t}, \hat{u})] - \frac{(m_1^2 + m_2^2)(2Y - \hat{s}\hat{s}_4)(\hat{s}_2 + \beta_Z \hat{s})}{4\hat{s}} D_{ZZ}^{1221}(\hat{t}, \hat{u}) \right. \\ &\quad \left. - 2m_1^2 m_Z^2 (\hat{s}_2 + \beta_Z \hat{s}) \left[ \frac{1}{\hat{u}_1} C_Z^{211}(\hat{u}) + \frac{1}{\hat{t}_1} C_Z^{211}(\hat{t}) \right] + m_1^2 [\hat{s}(m_1^2 - m_2^2) \right. \\ &\quad \left. - \hat{s}_2 m_Z^2 - \beta_Z \hat{s}(m_Z^2 + m_2^2 - m_1^2)] [D_{ZZ}^{1211}(\hat{s}, \hat{u}) + D_{ZZ}^{1211}(\hat{s}, \hat{t})] + (1 \leftrightarrow 2) \right\} , \end{aligned} \quad (\text{A.51})$$

<sup>13</sup>Notice that the present definition of  $E_1$  differs somewhat from the one employed in [30], where an analogous mixed case is also treated.

<sup>14</sup>For brevity we identify here  $m_j \equiv m_{\tilde{\chi}_j}$ .

$$A_{++++}^{(\tilde{\chi}_1\tilde{\chi}_22)}(\beta_Z, \hat{t}, \hat{u}; m_1^2, m_2^2) = \frac{8}{\hat{s}_4} \left\{ 2\beta_Z \hat{s} C_0^{111}(\hat{s}) + \frac{\hat{s}_4 + \beta_Z \hat{s}}{\hat{s}} E_2^{12}(\hat{t}, \hat{u}) - 2m_1^2 \hat{s}_4 \tilde{F}^{12}(\hat{s}, \hat{t}, \hat{u}) \right. \\ \left. + \frac{\hat{s}}{2} [\hat{s}_4 + \beta_Z (s_2 + 2m_2^2 - 2m_1^2)] [D_{ZZ}^{1211}(\hat{s}, \hat{u}) + D_{ZZ}^{1211}(\hat{s}, \hat{t})] + (1 \leftrightarrow 2) \right\}, \quad (\text{A.52})$$

$$A_{+-+-}^{(\tilde{\chi}_1\tilde{\chi}_21)}(\beta_Z, \hat{t}, \hat{u}; m_1^2, m_2^2) = \frac{16\hat{s}_2 Y}{\hat{s}_4 \hat{t}_1 \hat{u}_1} - \frac{4m_Z^2 \hat{s}(\hat{s}_2^2 - 2Y)}{\hat{s}_4 Y} [C_0^{111}(\hat{s}) + C_0^{222}(\hat{s})] \\ + \frac{4m_Z^2 \hat{s}_2 (2Y - \hat{s}\hat{s}_4)}{\hat{s}_4 Y} [C_{ZZ}^{121}(\hat{s}) + C_{ZZ}^{212}(\hat{s})] - \frac{4m_Z^2}{\hat{s}_4} \left\{ \frac{4(Y + 2\hat{u}m_Z^2)}{\hat{u}_1^2} B_Z^{12}(\hat{u}) \right. \\ \left. + \frac{(\hat{u}^2 + m_Z^4)}{Y} [E_1^{12}(\hat{s}, \hat{u}) + E_1^{21}(\hat{s}, \hat{u})] + (\hat{u} \leftrightarrow \hat{t}) \right\} \\ + \frac{4}{\hat{s}_4 Y} \left\{ \hat{s}(m_1^2 - m_2^2) [4(m_1^2 - m_2^2)(m_Z^2 + m_1^2 - m_2^2 - \hat{s}) + \hat{s}_2(\hat{s} + 2m_Z^2) - 2Y] C_0^{111}(\hat{s}) \right. \\ - (2Y - \hat{s}\hat{s}_4)(m_1^2 - m_2^2) [\hat{s} - 2(m_1^2 - m_2^2)] C_{ZZ}^{121}(\hat{s}) - 2\hat{s}(m_1^2 - m_2^2)^4 \tilde{F}^{12}(\hat{s}, \hat{t}, \hat{u}) \\ - \left( 2Y(m_1^4 - m_2^4)(m_1^2 - m_2^2) - (2Y - \hat{s}\hat{s}_4)m_Z^2 \left[ (m_1^2 - m_2^2)^2 + \frac{(m_1^2 + m_2^2)Y}{\hat{s}} \right] \right) D_{ZZ}^{1221}(\hat{t}, \hat{u}) \\ + \left[ \left( \frac{2\hat{u}_1}{\hat{s}} (m_1^2 - m_2^2) [\hat{u}_1(2m_Z^4 - 3m_Z^2 \hat{s} + \hat{u}\hat{s}_2) - (m_1^2 - m_2^2)\hat{s}(\hat{s} - 2\hat{u})] - \frac{4m_1^2 \hat{s}_2 Y^2}{\hat{s}\hat{u}_1} \right) C_Z^{211}(\hat{u}) \right. \\ - \left( (m_1^6 - m_2^6)\hat{s}(4\hat{u} - \hat{s}) - (m_1^2 - m_2^2)\hat{s}(m_Z^6 - \hat{u}\hat{u}_1^2 + m_Z^2 \hat{t}\hat{u} + 2m_Z^2 \hat{u}^2) \right. \\ \left. + m_1^2 m_2^2 (m_1^2 - m_2^2)(8\hat{u}_1^2 + 3\hat{s}^2 - 4\hat{s}\hat{u}) + (m_1^2 - m_2^2)^2 \hat{s}(\hat{s}m_Z^2 + 4\hat{u}\hat{u}_1) \right. \\ \left. - (m_1^4 - m_2^4)\hat{s}Y + 2Ym_1^2 [2(m_1^4 - m_2^4) + \hat{s}_2 m_Z^2] \right) D_{ZZ}^{1211}(\hat{s}, \hat{u}) + (\hat{u} \leftrightarrow \hat{t}) \left. \right\} \\ + (1 \leftrightarrow 2) \left. \right\}, \quad (\text{A.53})$$

$$A_{+-+-}^{(\tilde{\chi}_1\tilde{\chi}_22)}(\beta_Z, \hat{t}, \hat{u}; m_1^2, m_2^2) = \frac{8}{Y} \left\{ \hat{s} [2(m_1^2 - m_2^2) - \hat{s}_2] C_0^{111}(\hat{s}) + (2Y - \hat{s}\hat{s}_4) C_{ZZ}^{121}(\hat{s}) \right. \\ - \hat{s}(m_1^2 - m_2^2)^2 \tilde{F}^{12}(\hat{s}, \hat{t}, \hat{u}) - \frac{Y}{\hat{s}_4} [\hat{s}_4(m_1^2 + m_2^2) + Y] D_{ZZ}^{1221}(\hat{t}, \hat{u}) \\ \left. + [\hat{u} E_1^{12}(\hat{s}, \hat{u}) + 2(m_1^2 \hat{u}_1^2 + m_2^2 \hat{s}\hat{u}) D_{ZZ}^{1211}(\hat{s}, \hat{u}) + (\hat{u} \leftrightarrow \hat{t})] + (1 \leftrightarrow 2) \right\}, \quad (\text{A.54})$$

$$A_{++++}^{(\tilde{\chi}_1\tilde{\chi}_21)}(\beta_Z, \hat{t}, \hat{u}; m_1^2, m_2^2) = \frac{16Y}{\hat{s}_4} \left[ \frac{\hat{s}_2}{\hat{t}_1 \hat{u}_1} - \frac{m_Z^2}{\hat{s}^2} E_2^{12}(\hat{t}, \hat{u}) + \frac{m_Z^2}{\hat{t}_1^2} \left( \frac{2\hat{t}}{\hat{s}} - 1 \right) B_Z^{12}(\hat{t}) \right. \\ \left. + \frac{m_Z^2}{\hat{u}_1^2} B_Z^{12}(\hat{u}) \right] + \frac{8}{Y \hat{s}_4} \left( -m_1^2 [2(m_1^2 - m_2^2) - \hat{s}_2] (2Y - \hat{s}\hat{s}_4) C_0^{111}(\hat{s}) - m_1^2 \hat{s} \hat{s}_4^2 C_{ZZ}^{121}(\hat{s}) \right. \\ \left. + \frac{Y \hat{s}_4}{2\hat{s}} (m_1^2 + m_2^2) E_2^{12}(\hat{t}, \hat{u}) + m_1^2 (m_1^2 - m_2^2)^2 (2Y - \hat{s}\hat{s}_4) \tilde{F}^{12}(\hat{s}, \hat{t}, \hat{u}) \right)$$

$$\begin{aligned}
& + \frac{Y}{\hat{s}} \left[ Y[m_Z^2(m_1^2 + m_2^2) - 2m_1^2 m_2^2] + (m_1^4 + m_2^4)(Y - \hat{s}\hat{s}_4) \right] D_{ZZ}^{1221}(\hat{t}, \hat{u}) \\
& + \left\{ \frac{1}{\hat{s}\hat{u}_1} \left[ -\hat{u}_1^2(m_1^2 - m_2^2)^2(2Y - \hat{s}\hat{s}_4) + 2\hat{s}m_1^2[2m_Z^4(Y + 2\hat{u}^2) - \hat{u}^2\hat{s}_2^2] \right] C_Z^{211}(\hat{u}) \right. \\
& + m_1^2[-2(m_1^2 - m_2^2)(m_Z^4\hat{t} - 3m_Z^4\hat{u} - \hat{u}^2\hat{s}_2) + 2Y(m_Z^4 - m_1^2\hat{s}_4) \\
& \left. + (4m_Z^4 - \hat{s}_2^2)\hat{u}^2] D_{ZZ}^{1211}(\hat{s}, \hat{u}) + (\hat{u} \leftrightarrow \hat{t}) \right\} + (1 \leftrightarrow 2) \Big) , \tag{A.55}
\end{aligned}$$

$$A_{++++}^{(\tilde{\chi}_1\tilde{\chi}_2^2)}(\beta_Z, \hat{t}, \hat{u}; m_1^2, m_2^2) = 0 , \tag{A.56}$$

$$\begin{aligned}
A_{+-00}^{(\tilde{\chi}_1\tilde{\chi}_2^2)}(\beta_Z, \hat{t}, \hat{u}; m_1^2, m_2^2) = & -\frac{64m_Z^2 Y}{\hat{s}_4\hat{t}_1\hat{u}_1} + \frac{8\hat{s}m_Z^2(\hat{s}_2^2 - 2Y)}{\hat{s}_4 Y} [C_0^{111}(\hat{s}) + C_0^{222}(\hat{s})] \\
& - \frac{8m_Z^2\hat{s}_2(2Y - \hat{s}\hat{s}_4)}{\hat{s}_4 Y} [C_{ZZ}^{121}(\hat{s}) + C_{ZZ}^{212}(\hat{s})] + \left\{ \frac{8m_Z^2}{\hat{s}_4 Y} (\hat{u}^2 + m_Z^4) [E_1^{12}(\hat{s}, \hat{u}) + E_1^{21}(\hat{s}, \hat{u})] \right. \\
& \left. - \frac{32m_Z^2(\hat{u}^2 + m_Z^4)}{\hat{s}_4\hat{u}_1^2} B_Z^{12}(\hat{u}) + (\hat{u} \leftrightarrow \hat{t}) \right\} \\
& + \frac{2}{\hat{s}_4 Y m_Z^2} \left[ -\hat{s}[4\hat{s}(m_1^2 - m_2^2)^3 - 16m_1^2 m_Z^2(m_1^2 - m_2^2)(\hat{s} - m_Z^2) \right. \\
& + 4m_2^2(m_1^2 - m_2^2)(4m_Z^4 + \hat{s}\hat{s}_2) + 4(m_1^2 - m_2^2)m_Z^2(4m_Z^2\hat{s}_2 + \hat{s}_2^2 - 2Y) \\
& - (m_1^2 + m_2^2)\hat{s}_4(\hat{s}_2^2 - 2Y)] C_0^{111}(\hat{s}) - (2Y - \hat{s}\hat{s}_4)[(m_1^2 + m_2^2)(\hat{s}^2 + 8m_Z^4) + 2\hat{s}(m_1^2 - m_2^2)^2 \\
& - 2m_Z^2\hat{s}(5m_1^2 + m_2^2)] C_{ZZ}^{121}(\hat{s}) + \frac{1}{\hat{s}} \left\{ 2\hat{s}^3(m_1^2 - m_2^2)^4 + \hat{s}\hat{s}_2(\hat{s} - 8m_Z^2)Y(m_1^4 + m_2^4) \right. \\
& + (m_1^2 - m_2^2)(m_1^4 - m_2^4)\hat{s}^2(\hat{s}_4\hat{s}_2 + 2Y) - 4m_Z^2\hat{s}_2 Y^2(m_1^2 + m_2^2) + 2m_1^2 m_2^2 \hat{s}_2^2 Y \Big\} D_{ZZ}^{1221}(\hat{t}, \hat{u}) \\
& + \left\{ \frac{2}{\hat{s}\hat{u}_1} \left[ -2(m_1^2 - m_2^2)^2(\hat{u} - 2m_Z^2)\hat{u}_1^2\hat{s}^2 + 8m_1^2\hat{s}m_Z^2(m_Z^6\hat{t} + 5m_Z^6\hat{u} - 3m_Z^4\hat{t}\hat{u} \right. \right. \\
& - 7m_Z^4\hat{u}^2 + m_Z^2\hat{t}\hat{u}^2 + 5m_Z^2\hat{u}^3 - \hat{t}\hat{u}^3 - \hat{u}^4) + (m_1^2 + m_2^2)\hat{u}_1^2[8\hat{u}_1^2m_Z^4 + 5m_Z^4\hat{s}\hat{s}_2 \\
& - 2m_Z^2\hat{s}(2\hat{u}\hat{s}_2 + m_Z^4) + \hat{s}\hat{s}_4\hat{u}^2] \Big] C_Z^{211}(\hat{u}) + \left\{ 2\hat{s}^2(m_1^2 - m_2^2)^4 + m_2^6\hat{s}(\hat{s}^2 - 2m_Z^2\hat{s}_4 - 4\hat{s}\hat{u}) \right. \\
& - m_1^4m_2^2\hat{s}(\hat{s}^2 - 18\hat{s}m_Z^2 + 16\hat{u}m_Z^2 + 4\hat{s}\hat{u} - 8\hat{u}^2) + m_1^6\hat{s}[8m_Z^4 + \hat{s}(\hat{s} - 10m_Z^2) - 4\hat{u}_1^2] \\
& - m_1^2m_2^4\hat{s}(28m_Z^4 - 10m_Z^2\hat{t} + \hat{t}^2 - 34m_Z^2\hat{u} + 10\hat{t}\hat{u} + 13\hat{u}^2) - (m_1^2 - m_2^2)^2\hat{s}(8m_Z^6 \\
& - 5m_Z^4\hat{s} + 16m_Z^4\hat{u} + \hat{s}\hat{s}_2\hat{u} - 3\hat{s}\hat{u}^2) - 4m_1^4[4\hat{u}_1^2m_Z^4 + \hat{s}(\hat{u}^2 + m_Z^4)(\hat{s} - 7m_Z^2) \\
& + \hat{s}\hat{u}m_Z^2(10m_Z^2 - 3\hat{s})] - 4m_1^2m_2^2[m_Z^2(\hat{s} + 4m_Z^2)(\hat{u}^2 + m_Z^4) - 8m_Z^6\hat{u} - 5m_Z^2\hat{s}\hat{s}_2\hat{u} \\
& + \hat{s}^3\hat{u}] - m_2^2\hat{s}(-4m_Z^8 - 8m_Z^6\hat{u} + 5m_Z^4\hat{s}\hat{u} - 12m_Z^4\hat{u}^2 + \hat{s}\hat{u}^3) \\
& + m_1^2(16m_Z^6\hat{u}_1^2 - 12m_Z^8\hat{s} + 32m_Z^6\hat{s}\hat{u} - 5m_Z^4\hat{s}^2\hat{u} - 20m_Z^4\hat{s}\hat{u}^2 + 8m_Z^2\hat{s}\hat{u}^3 \\
& \left. \left. - \hat{s}^2\hat{u}^3) \right\} D_{ZZ}^{1211}(\hat{s}, \hat{u}) + (\hat{u} \leftrightarrow \hat{t}) \right\} + (1 \leftrightarrow 2) \Big] , \tag{A.57}
\end{aligned}$$

$$A_{+-00}^{(\tilde{\chi}_1\tilde{\chi}_2^2)}(\beta_Z, \hat{t}, \hat{u}; m_1^2, m_2^2) = \frac{2}{\hat{s}_4 Y m_Z^2} \left[ 2\hat{s}_4\hat{s}[2(m_1^2 - m_2^2)\hat{s}_2 - \hat{s}_2^2 + 2Y] C_0^{111}(\hat{s}) \right.$$

$$\begin{aligned}
& -2(6m_Z^2\hat{s} - 8m_Z^4 - \hat{s}^2)(2Y - \hat{s}\hat{s}_4)C_{ZZ}^{121}(\hat{s}) - 2[\hat{s}\hat{s}_2\hat{s}_4(m_1^2 - m_2^2)^2 + \hat{s}_4\hat{s}_2Y(m_1^2 + m_2^2) \\
& - 4m_Z^2Y^2]D_{ZZ}^{1221}(\hat{t}, \hat{u}) - 2\hat{s}_4\left\{(\hat{u}^2 + m_Z^4)E_1^{12}(\hat{s}, \hat{u}) + [(m_1^2 - m_2^2)^2\hat{s}\hat{s}_2 + m_2^2\hat{s}(2\hat{u}^2 + \hat{t}\hat{u} + m_Z^4) \right. \\
& \left. + m_1^2(4m_Z^2\hat{u}_1^2 - 3\hat{s}\hat{u}_1^2 - \hat{s}^2\hat{u})]D_{ZZ}^{1211}(\hat{s}, \hat{u}) + (\hat{u} \leftrightarrow \hat{t})\right\} + (1 \leftrightarrow 2) \Big] , \tag{A.58}
\end{aligned}$$

$$\begin{aligned}
A_{+++0}^{(\tilde{\chi}_1\tilde{\chi}_2^{11})}(\beta_Z, \hat{t}, \hat{u}; m_1^2, m_2^2) = & \frac{8(1 + \beta_Z)Y}{\hat{s}_4} \left[ -\frac{2(\hat{t} - \hat{u})}{\hat{t}_1\hat{u}_1} - \frac{2(m_Z^2\hat{s} - 2\hat{u}\hat{u}_1)}{\hat{s}\hat{u}_1^2} B_Z^{12}(\hat{u}) \right. \\
& + \frac{2(m_Z^2\hat{s} - 2\hat{t}\hat{t}_1)}{\hat{s}\hat{t}_1^2} B_Z^{12}(\hat{t}) + \frac{(\hat{t} - \hat{u})}{\hat{s}^2} E_2^{12}(\hat{t}, \hat{u}) \Big] + \frac{2}{\hat{s}_4m_Z^2} \left[ 2m_1^2(\hat{t} - \hat{u})[4(m_1^2 - m_2^2) \right. \\
& - (1 + \beta_Z)\hat{s}]C_0^{111}(\hat{s}) - \frac{(\hat{t} - \hat{u})}{2\hat{s}} \left\{ (m_1^2 - m_2^2)^2[4\hat{s}(m_1^2 + m_2^2) - (\hat{t} - \hat{u})^2] \right. \\
& + 4m_Z^2(m_1^2 + m_2^2)Y(1 + \beta_Z) + 4\beta_Zm_1^2m_2^2\hat{s}\hat{s}_4 - \beta_Z(m_1^2 + m_2^2)^2\hat{s}\hat{s}_4 \Big\} D_{ZZ}^{1221}(\hat{t}, \hat{u}) \\
& + \frac{\hat{s}_4(\hat{u} - \hat{t})(m_1^2 + m_2^2)(1 + \beta_Z)}{2\hat{s}} E_2^{12}(\hat{t}, \hat{u}) + \left\{ \frac{4}{\hat{s}\hat{u}_1} [-\hat{u}_1^2(\hat{u} - \hat{t})(m_1^2 - m_2^2)^2 \right. \\
& + 2(1 + \beta_Z)m_1^2m_Z^2\hat{s}(m_Z^4 - Y - \hat{u}^2)]C_Z^{211}(\hat{u}) - m_1^2[4(m_1^2 - m_2^2) \\
& - (1 + \beta_Z)\hat{s}][(\hat{u}_1^2 - m_2^2)(\hat{t} - \hat{u}) + m_Z^4 - Y - \hat{u}^2]D_{ZZ}^{1211}(\hat{s}, \hat{u}) - (\hat{u} \leftrightarrow \hat{t}) \Big\} \\
& \left. + (1 \leftrightarrow 2) \right] , \tag{A.59}
\end{aligned}$$

$$\begin{aligned}
A_{+++0}^{(\tilde{\chi}_1\tilde{\chi}_2^{22})}(\beta_Z, \hat{t}, \hat{u}; m_1^2, m_2^2) = & \frac{2(\hat{s}_4 + \beta_Z\hat{s})}{\hat{s}_4m_Z^2} \left[ 2(\hat{t} - \hat{u})C_0^{111}(\hat{s}) + \frac{(\hat{t} - \hat{u})}{\hat{s}} E_2^{12}(\hat{t}, \hat{u}) \right. \\
& + [(\hat{u}_1^2 - m_2^2)(\hat{u} - \hat{t}) + m_Z^4 - Y - \hat{t}^2]D_{ZZ}^{1211}(\hat{s}, \hat{t}) \\
& \left. - [(\hat{u}_1^2 - m_2^2)(\hat{t} - \hat{u}) + m_Z^4 - Y - \hat{u}^2]D_{ZZ}^{1211}(\hat{s}, \hat{u}) + (1 \leftrightarrow 2) \right] , \tag{A.60}
\end{aligned}$$

$$\begin{aligned}
A_{+-+0}^{(\tilde{\chi}_1\tilde{\chi}_2^{11})}(\beta_Z, \hat{t}, \hat{u}; m_1^2, m_2^2) = & -\frac{16Y(\hat{u} - \hat{t} - \hat{s}\beta_Z)}{\hat{s}_4\hat{t}_1\hat{u}_1} + \frac{8(\hat{u} - \hat{t} + \hat{s}\beta_Z)}{\hat{s}_4} [B_Z^{11}(\hat{s}) + B_Z^{22}(\hat{s})] \\
& - \frac{4\hat{s}}{\hat{s}_4Y} [(\hat{t} - \hat{u})(Y + \hat{u}^2 + \hat{t}^2) + \beta_Z(\hat{t}\hat{t}_1^2 + \hat{u}\hat{u}_1^2 - 2m_Z^2Y)][C_0^{111}(\hat{s}) + C_0^{222}(\hat{s})] \\
& + \frac{4}{\hat{s}_4Y} \{ (\hat{u} - \hat{t})\hat{s}_4(\hat{t}_1^2 + \hat{u}_1^2 + Y) - \beta_Z\hat{s}[\hat{t}\hat{t}_1(\hat{t} + m_Z^2) + \hat{u}\hat{u}_1(\hat{u} + m_Z^2) \\
& - 2m_Z^2Y] \} [C_{ZZ}^{121}(\hat{s}) + C_{ZZ}^{212}(\hat{s})] + \left\{ \frac{16}{\hat{s}_4\hat{u}_1^2} [m_Z^2Y - \hat{u}\hat{u}_1(\hat{u} + m_Z^2) - \beta_Z(m_Z^2Y - \hat{u}\hat{u}_1^2)] B_Z^{12}(\hat{u}) \right. \\
& - \frac{4}{\hat{s}_4Y} [m_Z^2Y - \hat{u}\hat{u}_1(\hat{u} + m_Z^2) + \beta_Z(\hat{u}\hat{u}_1^2 - m_Z^2Y)][E_1^{12}(\hat{s}, \hat{u}) + E_1^{21}(\hat{s}, \hat{u})] \\
& \left. - (\hat{u} \leftrightarrow \hat{t} \text{ , } \beta_Z \rightarrow -\beta_Z) \right\} + \frac{2}{m_Z^2\hat{s}_4Y} \left[ -4Y(m_1^2 - m_2^2)(\hat{u} - \hat{t} + \beta_Z\hat{s})B_Z^{11}(\hat{s}) \right.
\end{aligned}$$

$$\begin{aligned}
& +2\{(m_1^2 - m_2^2)(\hat{t} - \hat{u})[2\hat{s}(m_1^2 - m_2^2)(m_1^2 - m_2^2 + m_Z^2 - \hat{s}) + \hat{s}(Y + \hat{t}\hat{t}_1 + \hat{u}\hat{u}_1 + m_Z^2\hat{s}_2)] \\
& + m_1^2(\hat{t} - \hat{u})\hat{s}_4Y - \beta_Z\hat{s}[2\hat{s}(m_1^2 - m_2^2)^3 + 2(m_1^4 + m_2^4)(m_Z^2 - \hat{s})\hat{s} + 4m_1^4Y + 4m_1^2m_2^2(\hat{t}_1^2 \\
& + \hat{u}_1^2 + m_Z^2\hat{s} + Y) + (m_1^2 - m_2^2)(4m_Z^2\hat{u}_1^2 + \hat{s}^2\hat{s}_2 + 2\hat{s}\hat{u}(\hat{u} + \hat{s})) - m_2^2Y\hat{s}]\}C_0^{111}(\hat{s}) \\
& + 2(m_1^2 - m_2^2)\hat{s}(\hat{s} + 2m_2^2 - 2m_1^2)[\hat{u}(u + 2m_Z^2) - \hat{t}(\hat{t} + 2m_Z^2) + \beta_Z(2Y - \hat{s}\hat{s}_4)]C_{ZZ}^{121}(\hat{s}) \\
& - 2(m_1^2 - m_2^2)^4\hat{s}(\hat{t} - \hat{u} - \beta_Z\hat{s})\tilde{F}^{12}(\hat{s}, \hat{t}, \hat{u}) - \frac{Y}{2}\{(\hat{t} - \hat{u})[4(m_1^2 - m_2^2)(m_1^4 - m_2^4) \\
& - \hat{s}(m_1^2 - m_2^2)^2 - Y(m_1^2 + m_2^2)] - \beta_Z[8\hat{s}(m_1^2 - m_2^2)(m_1^4 - m_2^4) + (m_1^2 + m_2^2)Y\hat{s}_4 \\
& + (m_1^2 - m_2^2)^2(\hat{s}\hat{s}_4 + 4Y)]\}D_{ZZ}^{1221}(\hat{t}, \hat{u}) + \left[ -\frac{1}{\hat{u}_1}\left\{ -4\hat{u}_1^2(m_1^2 - m_2^2)^2(\hat{s}m_Z^2 - 2\hat{u}\hat{u}_1) \right. \right. \\
& + \hat{u}_1^2(m_1^2 - m_2^2)(8m_Z^6 + \hat{t}Y - 7m_Z^4\hat{u} - 8m_Z^2\hat{u}^2 + 3\hat{t}\hat{u}^2 + 4\hat{u}^3) + 2m_1^2(\hat{u} - \hat{t})(\hat{u} + m_Z^2)^2Y \\
& + \beta_Z\{4(m_1^2 - m_2^2)^2\hat{u}_1^3(\hat{s} - \hat{u}_1) + (m_1^2 - m_2^2)\hat{u}_1^2[4m_Z^2\hat{u}_1^2 - \hat{s}(\hat{u} + m_Z^2)^2 + \hat{s}\hat{u}(4\hat{u} - \hat{s})] \\
& - 2m_1^2Y[4m_Z^2\hat{u}_1^2 + \hat{s}(\hat{u} + m_Z^2)^2]\}\left. \right\}C_Z^{211}(\hat{u}) + \left\{ -2\hat{s}\hat{u}_1(\hat{s} + 4\hat{u})(m_2^6 - m_1^6 - m_1^4m_2^2 \right. \\
& - m_1^2m_2^4) - 4Ym_1^6(\hat{t} - \hat{u}) - 4m_1^2m_2^2(2m_1^2 - m_2^2)(\hat{s} - 2\hat{u}_1)(m_Z^2\hat{t}_1 + \hat{u}\hat{u}_1) \\
& + (m_1^2 - m_2^2)^2\hat{s}(4m_Z^6 + \hat{t}Y - 7m_Z^4\hat{u} + 2m_Z^2\hat{t}\hat{u} + 6\hat{u}^2\hat{u}_1 + \hat{t}\hat{u}^2) - m_1^2Y(m_1^2 - m_2^2)(8m_Z^2\hat{u}_1 \\
& + 10m_Z^2\hat{s} + 2\hat{s}\hat{u} - \hat{s}^2) - (m_1^2 - m_2^2)\hat{s}(-2m_Z^4Y - 6m_Z^6\hat{u} - \hat{t}\hat{u}Y + 3m_Z^4\hat{u}^2 + 6m_Z^2\hat{u}^3 \\
& - \hat{t}\hat{u}^3 - 2\hat{u}^4) + m_1^2Y(8m_Z^6 - 2m_Z^2\hat{t}\hat{u} + \hat{t}^2\hat{u} - 6m_Z^2\hat{u}^2 - \hat{u}^3) + \beta_Z\{2(m_2^6 - m_1^6 - m_1^4m_2^2 \\
& - m_2^4m_1^2)\hat{s}^2(m_Z^2 - 3\hat{u}) + 8\hat{s}Ym_1^6 - 4m_1^2m_2^2(2m_1^2 - m_2^2)\hat{s}\hat{u}_1(\hat{s} - 2\hat{u}_1) \\
& - 2(m_1^2 - m_2^2)^2\hat{s}\hat{u}_1(3\hat{u}_1^2 - Y) - m_2^2(m_1^2 - m_2^2)\hat{s}Y(6m_Z^2 - \hat{t} - 9\hat{u}) \\
& - 2(m_1^2 - m_2^2)\hat{u}_1^2(-m_Z^4\hat{s}_4 - 8m_Z^4\hat{u} + 3m_Z^2\hat{s}\hat{u} - \hat{s}^2\hat{u} + 4m_Z^2\hat{u}^2) \\
& \left. + m_2^2Y(8m_Z^2\hat{u}_1^2 - \hat{s}\hat{s}_4\hat{u})\right\}D_{ZZ}^{1211}(\hat{s}, \hat{u}) - (\hat{u} \leftrightarrow \hat{t} \text{ , } \beta_Z \rightarrow -\beta_Z) \Big] + (1 \leftrightarrow 2) \Big] , \quad (\text{A.61})
\end{aligned}$$

$$\begin{aligned}
A_{+-+0}^{(\tilde{\chi}_1\tilde{\chi}_2^{22})}(\beta_Z, \hat{t}, \hat{u}; m_1^2, m_2^2) = & -\frac{2(\hat{t} - \hat{u} + \beta_Z\hat{s})}{m_Z^2\hat{s}}\left\{ 2\hat{s}C_0^{111}(\hat{s}) + \frac{(\hat{s} + 4m_Z^2)Y}{\hat{s}_4}D_{ZZ}^{1221}(\hat{t}, \hat{u}) \right. \\
& \left. + E_1^{12}(\hat{s}, \hat{u}) + E_1^{12}(\hat{s}, \hat{t}) - (m_1^2 - m_2^2)\hat{s}[D_{ZZ}^{1211}(\hat{s}, \hat{u}) + D_{ZZ}^{1211}(\hat{s}, \hat{t})] + (1 \leftrightarrow 2) \right\} , \quad (\text{A.62})
\end{aligned}$$

$$\begin{aligned}
A_{++00}^{(\tilde{\chi}_1\tilde{\chi}_2^{21})}(\beta_Z, \hat{t}, \hat{u}; m_1^2, m_2^2) = & \frac{32m_Z^2}{\hat{s}_4}\left\{ \frac{2Y}{\hat{t}_1\hat{u}_1} - \frac{1}{\hat{s}\hat{u}_1^2}[2m_Z^2Y + (\hat{u} - \hat{t})(\hat{u}^2 - m_Z^4)]B_Z^{12}(\hat{u}) \right. \\
& - \frac{1}{\hat{s}\hat{t}_1^2}[2m_Z^2Y + (\hat{t} - \hat{u})(\hat{t}^2 - m_Z^4)]B_Z^{12}(\hat{t}) - \frac{Y}{\hat{s}^2}E_2^{12}(\hat{t}, \hat{u}) \Big\} + \frac{4}{\hat{s}_4m_Z^2}\left[ 2m_1^2[8m_Z^4 \right. \\
& - 2\hat{s}(m_1^2 - m_2^2) + \hat{s}\hat{s}_4]C_0^{111}(\hat{s}) + 2\hat{s}m_1^2(m_1^2 - m_2^2)^2\tilde{F}^{12}(\hat{s}, \hat{t}, \hat{u}) + \frac{(m_1^2 + m_2^2)\hat{s}_4m_Z^2}{\hat{s}}E_2^{12}(\hat{t}, \hat{u}) \\
& + \frac{1}{\hat{s}}\left\{ (m_1^4 + m_2^4)\hat{s}(\hat{t} + m_Z^2)(\hat{u} + m_Z^2) + 4(m_1^2 + m_2^2)m_Z^4Y + 2m_1^2m_2^2\hat{s}[Y + \hat{t}(\hat{t} + m_Z^2) \right. \\
& \left. + \hat{u}(\hat{u} + m_Z^2)] \right\}D_{ZZ}^{1221}(\hat{t}, \hat{u}) + \left\{ \frac{2}{\hat{u}_1}[8m_Z^6m_1^2 - \hat{u}_1^2(m_1^2 - m_2^2)^2]C_Z^{211}(\hat{u}) \right. \\
& \left. + 2m_1^2[m_1^2m_Z^2(4m_Z^2 - 3\hat{s}) + m_2^2(s_2^2 + \hat{s}m_Z^2) + 2\hat{s}_2m_Z^4]D_{ZZ}^{1211}(\hat{s}, \hat{u}) \right.
\end{aligned}$$

$$+(\hat{u} \leftrightarrow \hat{t}) \Big\} + (1 \leftrightarrow 2) \Big] , \quad (\text{A.63})$$

$$\begin{aligned} A_{++00}^{(\tilde{\chi}_1 \tilde{\chi}_2^2)}(\beta_Z, \hat{t}, \hat{u}; m_1^2, m_2^2) = & -\frac{4}{m_Z^2} \left[ 2\hat{s} C_0^{111}(\hat{s}) + \frac{2m_Z^2}{\hat{s}} E_2^{12}(\hat{t}, \hat{u}) \right. \\ & + (m_1^2 + m_2^2) \hat{s}_2 \tilde{F}^{12}(\hat{s}, \hat{t}, \hat{u}) - 2m_Z^2(m_1^2 - m_2^2) [D_{ZZ}^{1211}(\hat{s}, \hat{u}) + D_{ZZ}^{1211}(\hat{s}, \hat{t})] \\ & \left. + (1 \leftrightarrow 2) \right] , \quad (\text{A.64}) \end{aligned}$$

$$\begin{aligned} A_{+-+-}^{(\tilde{\chi}_1 \tilde{\chi}_2^1)}(\beta_Z, \hat{t}, \hat{u}; m_1^2, m_2^2) = & -\frac{16[\hat{s}_2 Y + \beta_Z m_Z^2 \hat{s}(\hat{u} - \hat{t})]}{\hat{s}_4 \hat{t}_1 \hat{u}_1} \\ & + \frac{8\hat{s}_2[Y - \hat{s}(\hat{s}_4 + \beta_Z(\hat{u} - \hat{t}))]}{\hat{s}_4 Y} [B_Z^{11}(\hat{s}) + B_Z^{22}(\hat{s})] - \frac{4\hat{s}\hat{s}_2}{\hat{s}_4 Y^2} [3m_Z^8 + (\hat{t}^2 + \hat{u}^2)(Y - 3m_Z^4) \\ & + \hat{t}^4 + \hat{t}^2 \hat{u}^2 + \hat{u}^4 - \beta_Z \hat{s}(\hat{t} - \hat{u})(\hat{t}^2 + \hat{t}\hat{u} + \hat{u}^2 - 2m_Z^4)] [C_0^{111}(\hat{s}) + C_0^{222}(\hat{s})] \\ & + \frac{4\hat{s}}{\hat{s}_4 Y^2} \left\{ -\hat{s}_4[(\hat{t}^2 - m_Z^4)^2 + (\hat{u}^2 - m_Z^4)^2 - (\hat{t}\hat{u} + m_Z^4)^2 + \hat{t}\hat{u}\hat{s}_2^2] \right. \\ & + \beta_Z(\hat{t} - \hat{u})[2Y^2 + (\hat{t}^2 + \hat{u}^2)(4Y + \hat{t}^2 + \hat{u}^2 - \hat{t}\hat{u}) - 2m_Z^4 \hat{t}\hat{u}] \left. \right\} [C_{ZZ}^{121}(\hat{s}) + C_{ZZ}^{212}(\hat{s})] \\ & - \left\{ 16 \left[ \left( \frac{m_Z^4(\hat{u} - \hat{t})}{\hat{s}_4 \hat{u}_1^2} - \frac{1}{2} \right) (1 - \beta_Z) + \frac{m_Z^2}{\hat{s}_4} \left( 1 - \frac{2m_Z^4}{\hat{u}_1^2} \right) - \frac{2\hat{u}\beta_Z}{\hat{s}_4} - \frac{\hat{u}^2}{Y\hat{s}_4} [\hat{s}_4 \right. \right. \\ & + \beta_Z(\hat{u} - \hat{t})] \left. \right] B_Z^{12}(\hat{u}) + \frac{2}{\hat{s}_4 Y^2} [\hat{s}_2(Y^2 - 2\hat{u}^3 \hat{s}_2) + 4m_Z^4 \hat{u}(Y + 2\hat{u}^2) \\ & - \beta_Z \hat{s}[Y^2 - 2\hat{u}^2(2m_Z^4 + \hat{u}\hat{s}_2)] \left. \right] [E_1^{12}(\hat{s}, \hat{u}) + E_1^{21}(\hat{s}, \hat{u})] + (\hat{u} \leftrightarrow \hat{t} \quad , \quad \beta_Z \rightarrow -\beta_Z) \left. \right\} \\ & + \frac{4}{\hat{s}_4 Y^2} \left[ -4Y(m_1^2 - m_2^2)[Y - \hat{s}(\hat{s}_4 + \beta_Z(\hat{u} - \hat{t}))] B_Z^{11}(\hat{s}) \right. \\ & - \hat{s} \left\{ (2Y - \hat{s}\hat{s}_4)(m_1^2 - m_2^2)^2 [2(m_1^2 - m_2^2) - 3\hat{s}_2] - (m_1^2 - m_2^2)[4\hat{s}_4 Y m_1^2 \right. \\ & + 2m_Z^4(2\hat{t}\hat{u} + m_Z^4) + (\hat{t}^2 + \hat{u}^2)(4\hat{t}\hat{u} - 10m_Z^4) + 4Y^2 + 3(\hat{t}^4 + \hat{u}^4)] + 2m_1^2 \hat{s}_4 \hat{s}_2 Y \\ & + \beta_Z(\hat{u} - \hat{t}) \{ \hat{s}(m_1^2 - m_2^2)^2 [3\hat{s}_2 - 2(m_1^2 - m_2^2)] - (m_1^2 - m_2^2)[4Y m_1^2 + \hat{s}(3(\hat{u}^2 + \hat{t}^2) \\ & + 4Y)] + 2\hat{s}_2 Y m_1^2 \} \left. \right\} C_0^{111}(\hat{s}) - \hat{s} \left\{ \hat{s}_4(m_1^2 - m_2^2)[4Y + 3(\hat{t} - \hat{u})^2](m_1^2 - m_2^2 - \hat{s}_2) \right. \\ & + 2m_1^2 \hat{s}_4^2 Y + \beta_Z(\hat{u} - \hat{t}) \{ (m_1^2 - m_2^2)[10Y + 3(\hat{t} - \hat{u})^2](m_1^2 - m_2^2 - \hat{s}_2) \\ & + 2m_1^2 \hat{s}_4 Y \} \left. \right\} C_{ZZ}^{121}(\hat{s}) + \frac{1}{\hat{s}} \{ 4m_1^2 m_2^2 m_Z^2 \hat{s} Y^2 + 2(m_1^4 + m_2^4) \hat{s}(3m_Z^2 - \hat{s}) Y^2 \\ & - (m_1^2 + m_2^2) \hat{s}_2 Y^3 + (m_1^2 - m_2^2)^4 \hat{s}^2 (2Y - \hat{s}\hat{s}_4) + 2(m_1^2 - m_2^2)(m_1^4 - m_2^4)(Y - \hat{s}\hat{s}_4) Y \hat{s} \\ & + \beta_Z \hat{s}(\hat{t} - \hat{u})(m_1^2 - m_2^2)^2 [\hat{s}^2(m_1^2 - m_2^2)^2 + 2(m_1^2 + m_2^2) Y \hat{s} + Y^2] \} D_{ZZ}^{1221}(\hat{t}, \hat{u}) \\ & + \left[ \frac{2}{\hat{s}\hat{u}_1} \left\{ \hat{s}\hat{u}_1^2(m_1^2 - m_2^2)^2 [Y(\hat{u}_1 - m_Z^2) + 3\hat{u}(\hat{u}^2 - 2m_Z^4) + 3\hat{t}m_Z^4] + (m_1^2 - m_2^2)\hat{u}_1^2 [2m_Z^8(\hat{s} - \hat{u}_1) \right. \right. \\ & \left. \left. - 2m_Z^6 \hat{u}(\hat{t} + \hat{t}_1) + 2m_Z^2 \hat{u}^2(\hat{u} - 2m_Z^2)^2 - \hat{s}\hat{u}^2(14m_Z^4 - \hat{s}^2 + 2m_Z^2 \hat{s} + 2\hat{u}\hat{s}_4) \right] \right. \end{aligned}$$

$$\begin{aligned}
& +2Ym_1^2[2m_Z^8(m_Z^2 - 4\hat{u}) + m_Z^2\hat{s}_4(m_Z^4\hat{s} + \hat{s}^2\hat{u} - 4m_Z^2\hat{u}^2) + 4m_Z^6\hat{u}(2\hat{s} - \hat{u}) + m_Z^2\hat{s}^2\hat{u}\hat{u}_1 \\
& + \hat{u}^3(2m_Z^2\hat{u} + \hat{s}^2 - 8m_Z^4)] - \beta_Z\hat{s}\{\hat{u}_1^3(m_1^2 - m_2^2)^2(Y + 3m_Z^2\hat{t}_1 + 3\hat{u}\hat{u}_1) \\
& + (m_1^2 - m_2^2)\hat{s}\hat{u}\hat{u}_1^2(4m_Z^4 - \hat{t}\hat{u} - 3\hat{u}^2) + 2m_1^2\hat{s}Y[\hat{u}\hat{u}_1(\hat{u} + m_Z^2) - m_Z^2Y]\}\}C_Z^{211}(\hat{u}) \\
& - \frac{1}{2}\left\{ -2\hat{s}(m_1^2 - m_2^2)^4(2Y - \hat{s}\hat{s}_4) + 4(m_1^6 - m_2^6)\hat{s}(m_Z^4\hat{t} - 5m_Z^4\hat{u} - \hat{s}_2\hat{t}\hat{u} + 2\hat{u}^3) \right. \\
& - 8Ym_1^6(Y - \hat{s}\hat{s}_4) + 4m_1^2m_2^2(m_1^2 - m_2^2)(2m_Z^8 - 14m_Z^6\hat{s} + 5m_Z^4\hat{s}^2 - 8m_Z^6\hat{u} + 26m_Z^4\hat{s}\hat{u} \\
& - \hat{s}^3\hat{u} + 12m_Z^4\hat{u}^2 - 10m_Z^2\hat{s}\hat{u}^2 + \hat{s}^2\hat{u}^2 - 8m_Z^2\hat{u}^3 - 2\hat{s}\hat{u}^3 + 2\hat{u}^4) + 8Ym_1^4m_2^2(Y - \hat{s}\hat{s}_4) \\
& + 6\hat{s}(m_1^2 - m_2^2)^2(m_Z^8 - 6m_Z^4\hat{u}^2 + \hat{t}^2\hat{u}^2 - 2\hat{u}^3\hat{s}_2) + 16Ym_1^4(-m_Z^2Y + m_Z^4\hat{t} - 3m_Z^4\hat{u} - \hat{u}^2\hat{s}_2) \\
& - 8Ym_1^2m_2^2(m_Z^4\hat{t} - 7m_Z^4\hat{u} + \hat{u}\hat{s}_2^2 - \hat{u}^2\hat{s}_2) + (m_1^2 - m_2^2)\hat{s}[-m_Z^8\hat{s}_2 - 10\hat{u}m_Z^4Y - 2m_Z^4\hat{t}^2\hat{u} \\
& + \hat{t}^3\hat{u}^2 - \hat{u}^3(4Y - 8\hat{s}\hat{s}_4 + \hat{t}^2)] + 2Ym_1^2[-m_Z^4(8Y + \hat{s}_2^2 + 16\hat{u}^2) + 6\hat{t}^2\hat{u}^2 + 9\hat{t}\hat{u}^3 + 4\hat{u}^4 + \hat{t}^3\hat{u}] \\
& - \beta_Z\hat{s}\{2\hat{s}(m_1^2 - m_2^2)^4(\hat{t} - \hat{u}) + 4\hat{s}(m_1^4 - m_2^4)(m_1^2 + m_2^2)(m_Z^4 + \hat{t}\hat{u} - 2\hat{u}^2) + 8Y(\hat{t} - \hat{u})m_1^6 \\
& - 32m_1^4m_2^2\hat{u}_1(\hat{u}\hat{u}_1 + m_Z^2\hat{t}_1) - 8m_1^2m_2^4(2m_Z^6 - 3m_Z^4\hat{s} + 6m_Z^2\hat{u}\hat{u}_1 + \hat{s}^2\hat{u} + 3\hat{s}\hat{u}^2 - 2\hat{u}^3) \\
& - (m_1^2 - m_2^2)[12\hat{s}\hat{u}(m_1^2 - m_2^2)(\hat{u}^2 - m_Z^4) + 16Ym_1^2(\hat{u}^2 - m_Z^4) + \hat{s}Y^2 + 4\hat{s}\hat{u}^2(Y \\
& + 2(\hat{u}^2 - m_Z^4))]\} - 2m_1^2Y[\hat{t}Y + \hat{u}(3Y + 4(\hat{u}^2 - m_Z^4))]\}\}D_Z^{1211}(\hat{s}, \hat{u}) \\
& + (\hat{u} \leftrightarrow \hat{t} \text{ , } \beta_Z \rightarrow -\beta_Z) \Big] + (1 \leftrightarrow 2) \Big] , \tag{A.65}
\end{aligned}$$

$$A_{+-+}^{(\tilde{\chi}_1\tilde{\chi}_2^2)}(\beta_Z, \hat{t}, \hat{u}; m_1^2, m_2^2) = \frac{8}{\hat{s}_4} \left\{ 2Y - \hat{s}[\hat{s}_4 + \beta_Z(\hat{t} - \hat{u})] \right\} D_Z^{1221}(\hat{t}, \hat{u}) . \tag{A.66}$$

## References

- [1] ALEPH, DELPHI, L3 and OPAL Collaborations, The LEP working group for Higgs boson searches, CERN-EP-2000-055; P. Igo-Kemenes, Search for New Particles and New Phenomena Results from  $e^+e^-$  Colliders, talk presented at XXXth International Conference on High Energy Physics, August 2000, Osaka, Japan, <http://ichep2000.hep.sci.osaka-u.ac.jp>
- [2] I.F. Ginzburg, G.L. Kotkin, V.G. Serbo and V.I. Telnov, Nucl. Instr. and Meth. **205**, 47 (1983); I.F. Ginzburg, G.L. Kotkin, V.G. Serbo, S.L. Panfil and V.I. Telnov, Nucl. Instr. and Meth. **219**,5 (1984); J.H. Kühn, E.Mirkes and J. Steegborn, Z. f. Phys. **C57**, 615 (1993).
- [3] Opportunities and Requirements for Experimentation at a Very High Energy  $e^+e^-$  Collider, SLAC-329(1928); Proc. Workshops on Japan Linear Collider, KEK Reports, 90-2, 91-10 and 92-16; P.M. Zerwas, DESY 93-112, Aug. 1993; Proc. of the Workshop on  $e^+e^-$  Collisions at 500 GeV: The Physics Potential, DESY 92-123A,B,(1992), C(1993), D(1994), E(1997) ed. P. Zerwas; E. Accomando *et.al.* Phys. Rep. **C299**, 299 (1998).
- [4] D.L. Borden, D.A. Bauer and D.O. Caldwell, Phys. Rev. **D48**, 1993 (4018); M. Bailargeon, G. Belanger and F. Boudjema, hep-ph/9405359; J.F. Gunion, in Perspectives on Higgs Particles, hep-ph/9705282.
- [5] M. Melles, hep-ph/0008125.
- [6] G. Jikia, S. Soldner-Rembold, Nucl.Phys.Proc.Suppl.**82**,373(2000), hep-ph/9910366, Int.Work. on High Energy Photon Colliders, DESY 2000.
- [7] E.W.N. Glover and J.J. van der Bij, Nucl. Phys. **B321**, 561 (1989).
- [8] G. Jikia Nucl. Phys. **B405**, 24 (1993).
- [9] G.J. Gounaris, J. Layssac, P.I. Porfyriadis and F.M. Renard, hep-ph/9909243, Eur. Phys. J. **C13**, 79 (2000).
- [10] M.S. Berger, M.S. Chanowitz, Nucl.Instrum.Meth.,**A355**,52(1995).
- [11] G.J. Gounaris, P.I. Porfyriadis, F.M. Renard, hep-ph/9812378, Phys. Lett. **B452**, 76 (1999), Phys. Lett. **B464**, 350 (1999) (E); G.J. Gounaris, P.I. Porfyriadis, F.M. Renard, hep-ph/9902230, Eur. Phys. J. **C9**, 673 (1999).
- [12] G.J. Gounaris, J. Layssac, P.I. Porfyriadis and F.M. Renard, hep-ph/9904450, Eur. Phys. J. **C10**, 499 (1999).
- [13] H. Nilles, Phys. Rep. **110**, 1 (1984); H.E. Haber, and G.L. Kane Phys. Rep. **117**, 75 (1985); J. Rosiek, Phys. Rev. **D41**, 3464 (1990), hep-ph/9511250(E); M. Kuroda, hep-ph/9902340.

- [14] J.F. Gunion, H.E. Haber, G. Kane and S. Dawson, "The Higgs Hunter's Guide", Addison-Wesley, Redwood City (1990).
- [15] A. Djouadi, V. Driesen, W. Hollik and J.I. Illana, Eur. Phys. J. **C1**, 163 (1998).
- [16] M.M. Mühlleitner, M. Krämer, M. Spira and P.M. Zerwas, talk at the International Workshop on High Energy Photon Colliders, June 14-17, 2000, DESY Hamburg, Germany, to appear in Nucl.Instr. & Meth. A.; M.M. Mühlleitner, Dissertation at the University of Hamburg, hep-ph/0008127; H. E. Haber *et.al.* hep-ph/0007006.
- [17] D.A. Dicus and C. Kao, Phys. Rev. **D49**, 1265 (1994).
- [18] G. Passarino and M. Veltman, Nucl. Phys. **B160**, 151 (1979).
- [19] K. Hagiwara, S. Matsumoto, D. Haidt and C.S. Kim, Z. f. Phys. **C64**, 559 (1995).
- [20] H. Haber, R. Hempling, prl6618151991; Y. Okada, M. Yamaguchi, T. Yanagida, Prog. Theor. Phys. **85**, 1 (1991); J. Ellis, G. Ridolfi, F. Zwirner, Phys. Lett. **B257**, 83 (1991); *ibid* Phys. Lett. **B262**, 477 (1991); R. Barbieri, M. Frigeni, Phys. Lett. **B258**, 395 (1991); S. Heinemeyer, W. Hollik and G. Weiglein, Phys. Lett. **B455**, 179 (1999), hep-ph/9903404.
- [21] G.J. Gounaris and G.P. Tsirigoti, Phys. Rev. **D56**, 3030 (1997), Phys. Rev. **D58**, 059901 (1998).
- [22] V. Telnov, hep-ex/0003024, hep-ex/0001029, hep-ex/9802003, hep-ex/9805002, hep-ex/9908005; I.F. Ginzburg, hep-ph/9907549; R. Brinkman hep-ex/9707017.
- [23] V. Telnov, talk at the International Workshop on High Energy Photon Colliders, <http://www.desy.de/gg2000>, June 14-17, 2000, DESY Hamburg, Germany, to appear in Nucl.Instr. & Meth. A.; D.S. Gorbunov, V.A. Il'yn, V.I. Telnov, hep-ph/0012175.
- [24] A. Djouadi, J. Kalinowski and M. Spira, HDECAY, hep-ph/9704448, Comput. Phys. Commun. **108**, 56 (1998).
- [25] A. Djouadi, S. Rosier-Lees (editors) *et.al.* "The Minimal Supersymmetric Standard Model: Group Summary Report", hep-ph/9901246; V. Barger *et.al.* "Report of SUGRA Working Group for Run II of the Tevatron", hep-ph/0003154.
- [26] G.-C. Cho, K. Hagiwara, Nucl. Phys. **B574**, 623 (2000).
- [27] C. Quigg, Talk dedicated to the memory of Sam Treiman, hep-ph/0001145.
- [28] M. Jacob and G.C. Wick, Ann. Phys. (N.Y.) **7**, 404 (1959).
- [29] G.J. Gounaris, J. Layssac and F.M. Renard, hep-ph/0003143, Phys. Rev. **D62**, 073013 (2000).

- [30] G.J. Gounaris and P.I. Porfyriadis, hep-ph/0007110, to appear in Eur. Phys. J. C.

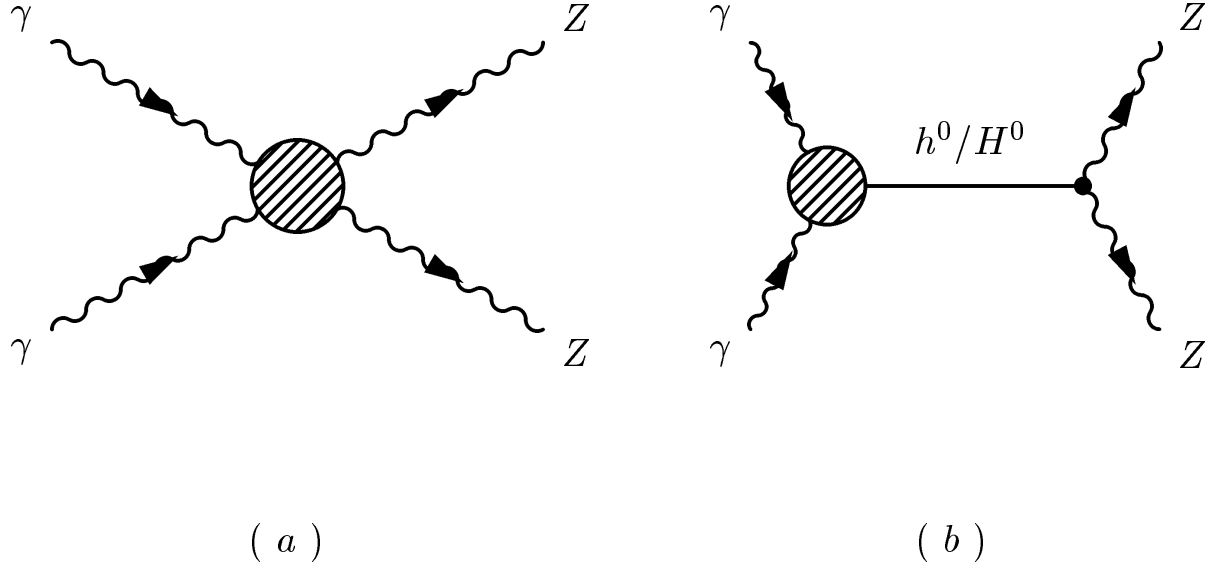


Figure 1: Feynman Diagrams for the  $\gamma\gamma \rightarrow ZZ$  process in SM and MSSM models.

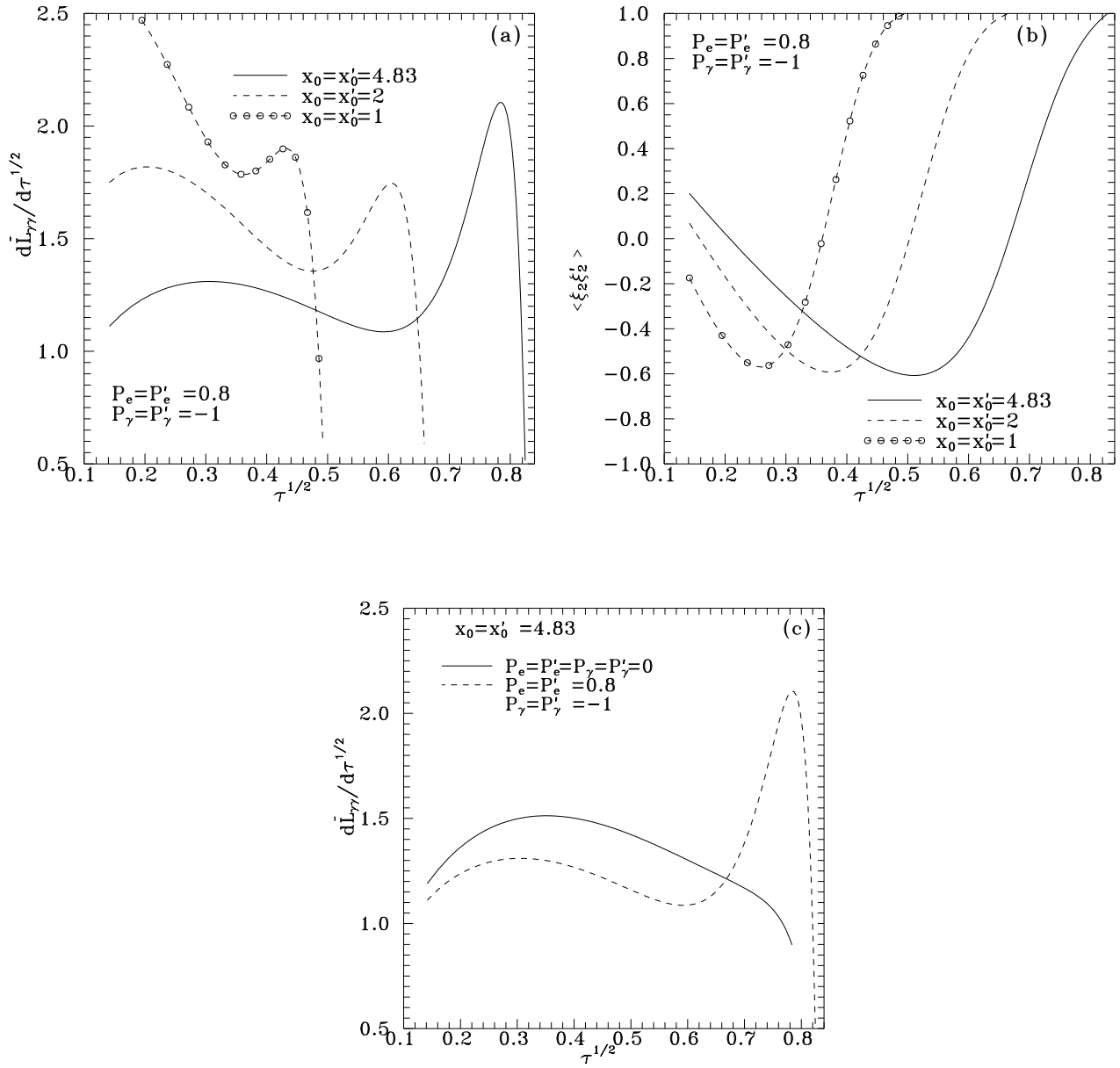


Figure 2: Photon-photon luminosity factor (a), and circular polarization factor (b), for longitudinally polarized  $e^\pm$  beams and circularly polarized laser photons; while (c) gives the same luminosity factor for unpolarized  $e^\pm$  beams and laser photons. The laser parameters  $x_0, x'_0$ , are indicated in the figures.

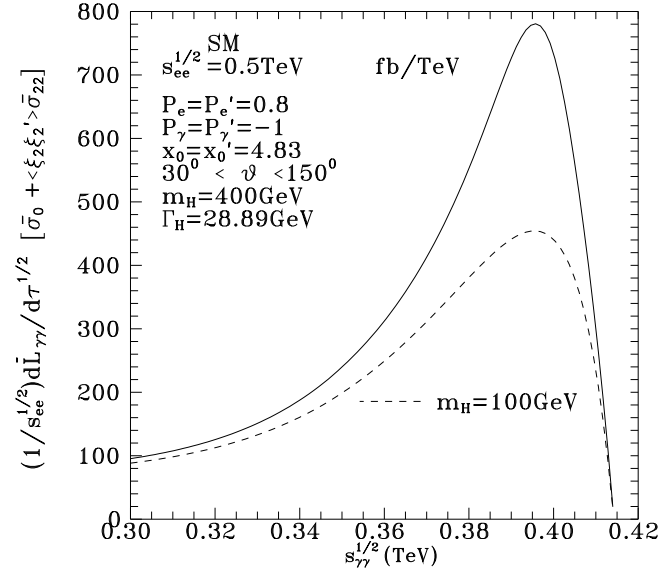


Figure 3: A 0.5 TeV Linear Collider picture of the SM contribution to the  $\sigma(\gamma\gamma \rightarrow ZZ)_{\text{Laser}}$  cross section for a standard Higgs with  $m_H = 400$  GeV. The dash lines give the results for  $m_H = 100$  GeV. The machine is assumed to run at 0.5 TeV total  $e^-e^+$  energy using the polarizations and  $x_0, x'_0$  values indicated in the figure.

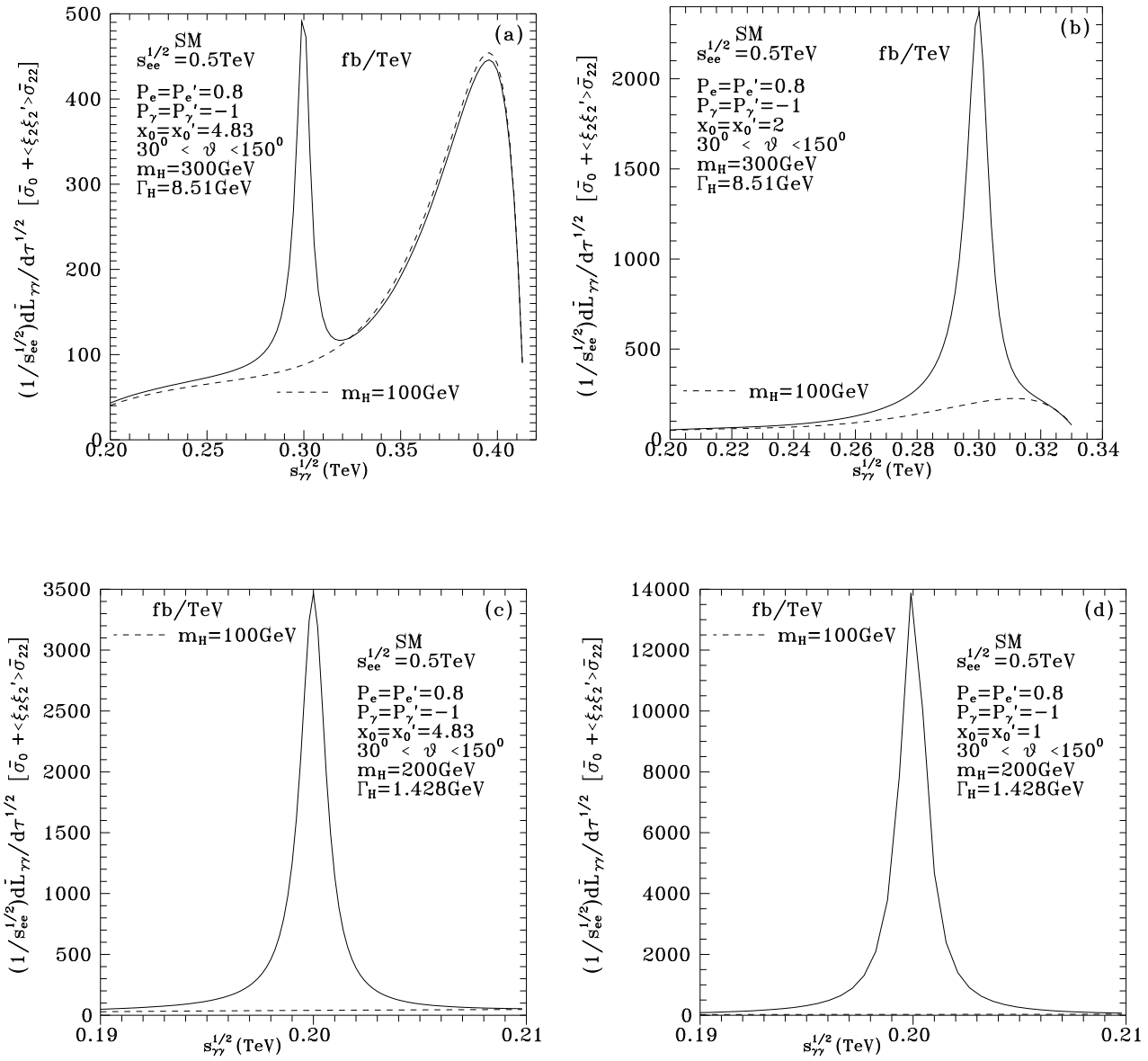


Figure 4: A 0.5 TeV Linear Collider picture of the SM contribution to the  $\sigma(\gamma\gamma \rightarrow ZZ)_{\text{Laser}}$  cross section for a standard Higgs with  $m_H = 300$  GeV (a, b) and  $m_H = 200$  GeV (c, d). The dash lines give the results for  $m_H = 100$  GeV. The machine is assumed to run at 0.5 TeV total  $e^-e^+$  energy using the polarizations and  $x_0, x_0'$  values indicated in the figures.

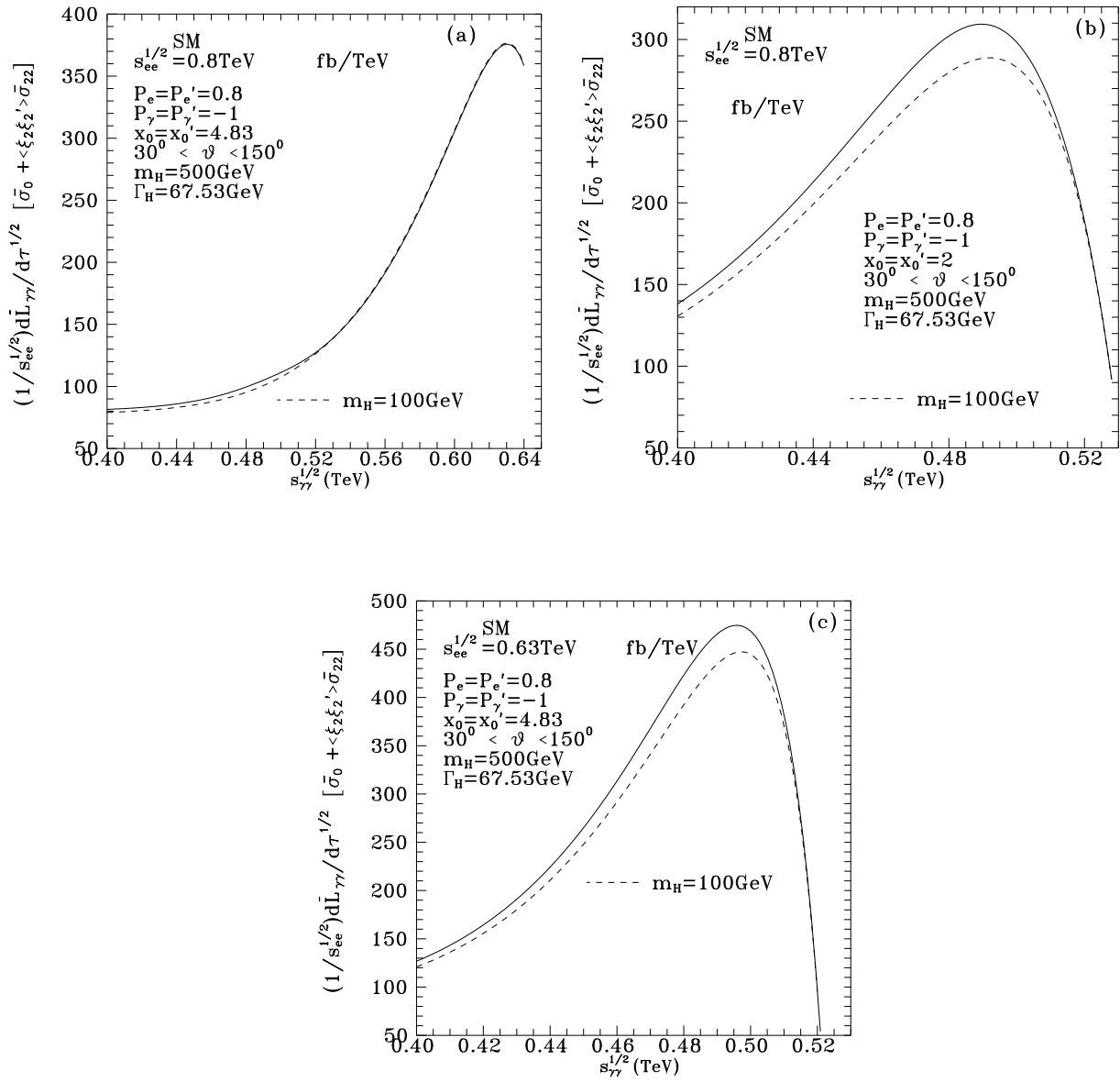


Figure 5: A 0.8 TeV Linear Collider picture of the SM contribution to the  $\sigma(\gamma\gamma \rightarrow ZZ)_{\text{Laser}}$  cross section for a standard Higgs with  $m_H = 500$  GeV. The dash lines give the results for  $m_H = 100$  GeV. In (a), (b) the machine is assumed to run at 0.8 TeV total  $e^-e^+$  energy using the indicated polarizations and  $x_0, x_0'$  values; while in (c) the machine is tuned at a total  $e^-e^+$  energy of 0.63 TeV.

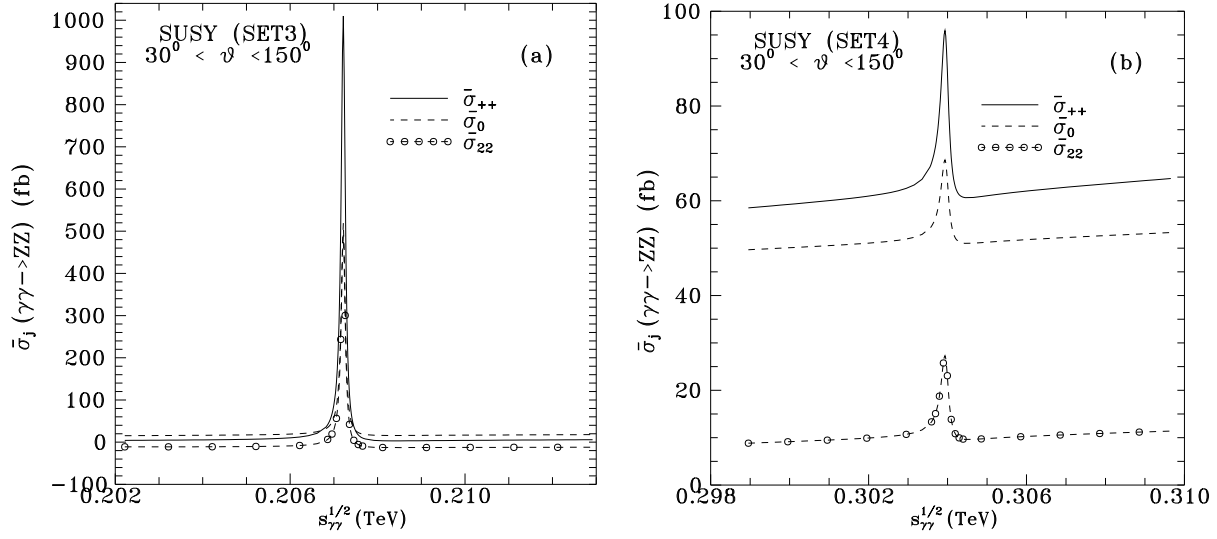


Figure 6: SUSY predictions for the cross sections  $\bar{\sigma}_0(\gamma\gamma \rightarrow ZZ)$ ,  $\bar{\sigma}_{22}(\gamma\gamma \rightarrow ZZ)$  and  $\bar{\sigma}_{++}(\gamma\gamma \rightarrow ZZ)$  in the  $H^0$  mass region, using the parameters of Set3 (a) and Set4 (b) in Table 2; see text.